This manuscript is a pre-print that has been accepted for publication in Tectonics.

Terrane boundary reactivation, barriers to lateral fault propagation and reactivated fabrics - Rifting across the Median Batholith Zone, Great South Basin, New Zealand

Thomas B. Phillips*; Ken J. McCaffrey

Department of Earth Sciences, University of Durham, Science labs, Elvet Hill, Durham, DH1 3LE

***thomas.b.phillips@durham.ac.uk**

Key points

- We document multiple styles of structural inheritance that influence various aspects of rift physiography in the Great South Basin, New Zealand
- The southern boundary of the Median Batholith Zone terrane is reactivated as a large extensional shear zone and detachment
- Faults splay, segment and eventually terminate as they approach stronger material associated with a granitic laccolith.

Abstract

Prominent pre-existing structural heterogeneities within the lithosphere may localise or partition deformation during tectonic events. The NE-trending Great South Basin, offshore New Zealand, formed perpendicular to a series of underlying crustal terranes, including the dominantly granitic Median Batholith Zone, which along with the boundaries between individual terranes, exert a strong control on rift physiography and kinematics. We find that the crustal-to-lithospheric scale southern terrane boundary of the Median Batholith Zone is associated with a crustal-scale shear zone that was reactivated during Late Cretaceous extension between Zealandia and Australia. This reactivated terrane boundary is oriented at a high-angle to the faults defining the Great South Basin. We identify a large granitic laccolith along the southern margin of the Median Batholith, expressed as sub-horizontal packages of reflectivity and acoustically transparent areas on seismic reflection data. The presence of this strong granitic body inhibits the lateral south-westward propagation of NE-trending faults, which segment into a series of splays that rotate to align along the margin as they approach. Further, we also identify two E-W and NE-SW oriented basement fabrics, likely corresponding to prominent foliations, which are exploited by small-scale faults across the basin. We show that different mechanisms of structural inheritance are able to operate simultaneously, and somewhat independently, within rift systems at different scales of observation. The presence of structural heterogeneities across all scales need to be incorporated into our understanding of the structural evolution of complex rift systems.

1. Introduction

Continental crust is highly heterogeneous. It is comprised of distinct crustal units, including island arcs, exotic terranes and igneous plutons, the boundaries between which may represent pronounced rheological and lithological contrasts, forming crustal-to-lithospheric scale structures. Individual crustal units likely contain numerous pre-existing structural heterogeneities reflective of their own unique histories prior to amalgamation into the continental crust as well as structures formed during subsequent tectonic events (Howell 1980; McWilliams & Howell 1982; Bishop et al. 1985; Mortimer 2004; Lundmark et al. 2013; Peace et al. 2017; Johnston 2019). Accordingly, a range of pre-existing heterogeneities are present throughout the crust across all scales, and may exert a considerable influence over multiple aspects of rift physiography during continental extension.

Lithosphere-scale structures often localise strain, as indicated by tectonic events repeatedly localising in highly deformed orogenic belts surrounding more stable cratonic continental interiors. These belts may control the location of rift systems and, to some extent, continental breakup (e.g. Wilson 1966; Ring 1994; Dore et al. 1997; Tommasi & Vauchez 2001; Thomas 2006; Paton et al. 2016; Wenker & Beaumont 2016; Phillips et al. 2018; Thomas 2018; Heron et al. 2019). The distribution of different crustal rheologies and their associated strength variations, such as between distinct crustal terranes or between igneous batholiths and adjacent terranes, may inhibit fault nucleation and propagation in some areas whilst promoting it in others (Critchley 1984; Koopmann et al. 2014; Magee et al. 2014; Peace et al. 2017; Howell et al. 2019). Pre-existing structures in the crust may also localise deformation and control the geometry and evolution of fault and rift systems (e.g. Daly et al. 1989; Fossen et al. 2016; Mortimer et al. 2016; Phillips et al. 2016; Fazlikhani et al. 2017; Morley 2017; Peace et al. 2017; Dawson et al. 2018; Rotevatn et al. 2018b; Vasconcelos et al. 2019). In addition, pre-existing structures and fabrics at outcrop scale may be exploited by and control the geometry of later faults and fractures (Morley et al. 2004; Paton & Underhill 2004; De Paola et al. 2005; Morley 2010; Chattopadhyay & Chakra 2013; Kirkpatrick et al. 2013; Duffy et al. 2015; Dichiarante et al.

2016; Mortimer et al. 2016; Phillips et al. 2017). Equally, pre-existing structures do not always influence rift physiography; some may remain passive during subsequent tectonic events, whilst certain structures may only be selectively reactivated (e.g. Roberts & Holdsworth 1999; Reeve et al. 2013). Numerous examples of interactions between pre-existing structures and rift-related faults have been documented in rift systems worldwide; however, we often lack an in-depth understanding of the mechanics of these interactions, as well as how different scales of pre-existing structure may influence different aspects of rift geometry and development.

In this study, we focus on the Great South Basin, a NE-trending rift system located offshore of the South Island of New Zealand. Basement beneath the basin comprises a series of volcano-sedimentary terranes, which accreted along the southern margin of Gondwana during protracted Cambrian-Cretaceous subduction (Mortimer et al. 1999; Tulloch et al. 1999; Mortimer 2004, 2014; Robertson et al. 2019; Robertson & Palamakumbura 2019; Tulloch et al. 2019). These terranes are separated by W- to WNW-trending crustal-to-lithospheric scale boundaries that are oriented perpendicular to the overlying basin (Muir et al. 2000; Mortimer et al. 2002). The presence of prominent terrane boundaries, strength variations between different terranes and various heterogeneities within individual terranes, make this the ideal location to analyse multiple structural heterogeneities and their interactions with rift-related faults, across a range of spatial scales. We focus on the evolution of the basin atop the Median Batholith Zone, a Carboniferous-Early Cretaceous Cordilleran-style magmatic arc, and its boundaries with the Western Province terranes to the south and the Brook Street and Murihiku Terranes to the north (Figure 1) (Bishop et al. 1985; Tulloch et al. 1999; Mortimer et al. 2002; Jongens 2006; Tulloch et al. 2019).

Using borehole-constrained 2D and 3D seismic reflection data, we document multiple structural heterogeneities beneath the Great South Basin, and determine how they influence rift physiography and kinematics. . The styles of structural inheritance established in this study and their associated characteristic fault geometries; may be indicative of similar styles of structural inheritance present in other rift systems worldwide.

2. Regional geological setting and evolution

The Great South Basin is a NE-trending Late Cretaceous rift basin located offshore of the east coast of the South Island of New Zealand. It contains a maximum sedimentary thickness of 8.6 km, which includes up to 4 km of Upper Cretaceous strata (Beggs 1993; Sahoo et al. 2014; Morley et al. 2017) (Figure 1, 3). The Great South Basin, along with the adjacent Canterbury Basin and Bounty Trough, is situated within the Campbell Plateau, a submerged (<1000 m water depth) area of thinned continental crust (22-32 km) that extends ~1000 km southeast of the South Island (Figure 1) (Beggs 1993; Mortimer et al. 2002; Grobys et al. 2009; Uruski 2010; Higgs et al. 2019). Here, we focus on a 21,000 km^2 area covering the southern part of the Great South Basin, located to the southeast of Stewart Island (Figure 1).

The basement geology of New Zealand comprises a series of crustal to lithospheric terranes that accreted to the southern margin of Gondwana during protracted subduction from the Cambrian-Early Cretaceous (e.g. Bishop et al. 1985; Bradshaw 1989; Muir et al. 2000; Mortimer 2014; Mortimer et al. 2014). Subduction ceased during the Early Cretaceous (~105 Ma) as the buoyant Hikurangi Plateau collided along the margin (Davy et al. 2008; Uruski 2015). Since the Cenozoic, these terranes have been offset along the Alpine Fault, a major plate boundary and strike-slip fault located along the spine of the South Island that has accommodated >450 km, and potentially >700 km, offset (Wellman 1953; Cooper et al. 1987; Sutherland et al. 2000; Lamb et al. 2016). Due to this offset, the basement terranes of the South Island are also present beneath the North Island (Figure 1) (Muir et al. 2000; Mortimer et al. 2002; Collanega et al. 2018). The basement terranes, which together comprise the Austral Superprovince, are divided into Eastern and Western provinces separated by the Median Batholith Zone (Mortimer et al. 2014). The timing of accretion along the Gondwana margin becomes younger eastwards, with those terranes of the Western Province terranes accreting to the margin of Gondwana earlier than those in the Eastern Province and occupying a more proximal position with respect to the continental interior. Here, we focus on terranes that underlie the Great South Basin; i.e. the Western

Province Terranes, the Median Batholith Zone and the Brook Street and Murihiku terranes of the Eastern Province (Figure 1).

The Western Province comprises the Buller and Takaka terranes, dominantly (meta)-sedimentary Gondwana-derived continental fragments that accreted along the margin during the Cambrian-Devonian (Bradshaw 1989; Mortimer 2004; Bache et al. 2014; Tulloch et al. 2019). The Eastern Province terranes largely originated within the Panthalassa Ocean as a series of volcanic and magmatic arcs and associated sedimentary basins (Bishop et al. 1985; Mortimer et al. 1997; Mortimer et al. 2002; Mortimer 2004). The Brook Street terrane is immediately north of the Median Batholith and comprises a Permian volcanic and volcaniclastic sequence that initially formed as an intra-oceanic arc (Landis et al. 1999; Mortimer 2004). Further north, the Murihiku terrane is composed of gently folded Jurassic-aged sandstones and volcaniclastic rocks that were initially part of a forearc sedimentary basin (Campbell et al. 2003; Mortimer 2004). Between the Western and Eastern Province terranes is the Median Batholith Zone, a Cordilleran-style magmatic arc that represented the site of subduction-related magmatism from 375-110 Ma (Mortimer et al. 1999; Mortimer 2004). Although previously interpreted as a highly tectonised allocthonous zone, recent studies have demonstrated that the majority of plutonic material is autochthonous, with only relatively minor reworking and tectonism identified, and is therefore referred to as the Median Batholith Zone in this study (Mortimer et al. 1999). The Median Batholith Zone comprises numerous plutonic intrusions that can be divided into various suites based on the age of emplacement and composition (Tulloch 1988; Allibone & Tulloch 2004). Based on well information and onshore exposures at Stewart Island, an overall southwards younging trend occurs across the batholith, with the Cretaceous-aged Separation Point Batholith suite located along the southern margin and older batholith suites further north (Mortimer et al. 1999; Muir et al. 2000; Allibone & Tulloch 2004; Tulloch et al. 2019).

The Great South Basin formed via two phases of Late Cretaceous extension related to the breakup of Gondwana. Extensional activity may have begun in the Jurassic-Early Cretaceous in a back-arc setting along the southern margin of Gondwana, with Jurassic strata identified in the deepwater Taranaki Basin and potentially in the Great South Basin (Grobys et al. 2007; Uruski et al. 2007;

Uruski 2010). Initial NE-SW oriented extension occurred between Australia and the contiguous Zealandia and Western Antarctica at ~101-89 Ma related to the opening of the Tasman Sea and the northwards propagation of the Tasman ridge (Kula et al. 2007; Kula et al. 2009; Sahoo et al. 2014; Tulloch et al. 2019). A second rift phase, related to the breakup of Zealandia and Western Antarctica and associated with the eventual formation of the Pacific-Antarctic ridge, occurred from 90-80 Ma (Kula et al. 2007; Tulloch et al. 2019). The regional extension direction was oriented NW-SE, roughly parallel to the underlying basement terrane boundaries, and resulted in the formation of the NE-trending Great South Basin (Figure 1). Late Cretaceous extension, forming the Great South and Canterbury basins and the Bounty Trough reduced crustal thickness to 22-32 km across the area (Mortimer et al. 2002). In the Great South Basin, faults related to this activity have been proposed to sole out onto a mid-crustal detachment (Uruski et al. 2007; Sahoo et al. 2014).

The onset of subduction in the Tonga-Kermadec region in the Oligo-Miocene and the formation of the Alpine Fault resulted in a regional compressional regime across New Zealand (Cooper et al. 1987; Sutherland et al. 2000; Sutherland et al. 2010; Bache et al. 2012). The Great South Basin was relatively far-removed from the compressional stresses associated with the formation of this new plate boundary, with regional compression expressed as low-amplitude, long wavelength folding (Uruski 2010).

3. Data and Methods

3.1 Seismic interpretation

We use borehole-constrained 2D and 3D seismic reflection data, covering an area of 21,000 km^2 offshore of the South Island of New Zealand. A 3D seismic reflection volume (GSB-3D) was acquired in the south of this area and covers ~1,400 km^2 (Figure 1). Seismic reflection data follow the SEG normal polarity convention; that is, a downwards increase in acoustic impedance (i.e. the seabed) is represented by a peak, whereas a downwards decrease in acoustic impedance is represented by a trough (see seabed inset in Figure 2b). 2D seismic reflection data record to 6-8 s TWT and display variable image quality between individual surveys. Typical spacing between individual 2D seismic sections outside of the 3D volume is ~3 km, although this increases to ~9 km south of the 3D volume. The 3D seismic volume records to 8 s TWT and displays excellent image quality throughout. Using a velocity of ~2800 m/s (based on interval velocities derived from the Pukaki-1 well) and a frequency of 20 Hz, we calculate a vertical resolution (wavelength (λ)/4) of ~35 m across the 3D volume within the Cretaceous interval. This represents roughly a minimum vertical resolution within this interval.

We mapped a series of prominent seismic reflections throughout the dataset and linked them to the regional stratigraphy (Figure 2). The ages of regional stratigraphic horizons were constrained by the nearby Pukaki-1, Pakaha-1, Tara-1, Toroa-1 and Rakiura-1 boreholes (Figure 1). A seismic-well tie was performed on the Pukaki-1 well to link the seismic interpretations to the well data (Figure 2). Top Acoustic Basement and intra-Upper Cretaceous horizons form the main surfaces referred to throughout this study, as they were the most affected by rift activity (Figure 2). Top Acoustic Basement typically represents top crystalline basement across the area (Figure 1), although in some instances coherent reflectivity suggestive of sedimentary layering is observed beneath this surface, potentially related to earlier, likely Jurassic, rifting (Uruski et al. 2007) (Figure 3). The intra-Upper Cretaceous horizon was interpreted throughout the 3D seismic volume and across the main basin depocentre to map syn-rift fault geometries in more detail (Figure 1, 3). Seismic interpretations were carried out, and are presented, in the time domain (seconds Two-way-travel time; s TWT). Key structural measurements were converted to the depth domain based on regional checkshot information (see supplementary material for checkshot data).

Crystalline basement in the area is mostly associated with the underlying Median Batholith (Figure 1). Based on U-Pb zircon ages, the Pakaha-1 well penetrates a Carboniferous granitic basement (323 Ma) (Tulloch et al. 2019), and the Pukaki-1 well penetrates a Cretaceous-aged granitic basement to the southeast (Figure 1). The Pukaki-1 granite is dated at 107 Ma and can be confidently correlated with the Separation Point Batholith suite (Tulloch et al. 2009; Tulloch et al. 2019). The Separation Point Batholith suite is also identified in the same structural setting, to the south of the Median Batholith

Zone, along its boundary with the Western Province terranes, in the North Island (Muir et al. 2000), suggesting it occupies a similar structural setting along the length of the batholith.

3.2 Quantitative fault analysis

We performed quantitative analyses, in the form of throw-length plots, on a series of faults within the basin to quantify their geometric and kinematic evolution. The geometry of each fault analysed, including horizon cutoffs and any tip lines were carefully constrained throughout the data to minimise any interpretation-related artefacts (Walsh et al. 2003; Duffy et al. 2015). We measure fault throw as opposed to displacement to avoid errors associated with depth conversion during the measurement of displacement. Based on our fault interpretations we calculated throw-length plots for individual fault segments at both the Acoustic Basement and intra-Upper Cretaceous stratigraphic horizons. To accurately constrain the kinematic evolution of a fault we need to record all fault slip-related strain, including both brittle faulting and ductile folding such as that associated with fault propagation folding. Therefore, where necessary, horizon cut-offs were projected to the fault plane from an area unaffected by local fault parallel folding (e.g. Walsh et al. 1996; Long & Imber 2012; Whipp et al. 2014; Duffy et al. 2015; Coleman et al. 2018). Throw measurements were taken for each fault along a series of parallel seismic sections within the 3D volume, oriented orthogonal to the main fault trend and each separated by ~340 m. Analyses of individual faults were then projected onto a single plane representing a strike projection of the overall fault system. This allowed us to calculate the cumulative throw accrued across the fault system and to analyse how strain was accommodated along its length.

4. Rift physiography and basement structure

4.1 Regional rift geometry

The Great South Basin is characterised by NE-trending, predominantly SE-dipping faults. NW-dipping faults are also present and help define a series of NE-trending basement ridges in the east of the area (Figure 1). The centre of the basin reaches 3-4 s TWT (~4.5 km) depth and shallows eastwards onto the continental shelf (~1.5 s TWT, ~1.3 km) (Figure 1, 3). The basin deepens to around 5 s TWT (~9 km) in the north and the south (Figure 1).

Upper Cretaceous strata display divergent wedges and thicken towards the hanging walls of major NE-trending faults (Figure 3), indicating Late Cretaceous fault activity. We also recognise a potentially earlier phase of activity, with apparent syn-rift strata present below the acoustic basement surface in the hangingwalls of some structures (Figure 3). Although we are unable to assign an age to these strata, we suggest that, based on regional considerations, they are likely Late Jurassic-Cretaceous in age (Uruski et al. 2007; Uruski 2010). Palaeocene to recent strata comprise the post-rift basin fill and display a slight westwards thickening related to increased sediment input and clinoform progradation from the mainland (Figure 3). This large clinoform sequence forms a major bathymetric escarpment to the west (Figure 3). E-dipping faults along the western margin of the basin appear to potentially merge at depth (Figure 3). In the east of the area, the Pakaha-1 well penetrates granitic basement atop a ~10 km wide NE-trending horst termed the Pakaha Ridge (Figure 1, 3). Basement beneath this ridge is highly reflective and appears to dip westwards. A series of W-dipping faults define the western margin of the Pakaha ridge and merge with the basement reflectivity at ~5-6 s TWT (~10.5 km) (Figure 3). A ~65 km long, SSW-dipping fault is located in the south of the study area (Figure 1). This fault is co-located along the along-strike projection of the boundary between the Median Batholith and Western Province terranes (Figure 1), and is therefore termed the Terrane Boundary Fault.

4.2 Basement structures

The Terrane Boundary Fault records >1 s TWT (>2 km) throw across the Acoustic Basement surface (Figure 4, 5). This fault corresponds to a prominent reflection on seismic data, with a package of high-amplitude fault-parallel reflections present in basement in its immediate footwall (Figure 4, 5). This reflection package is truncated by the top Basement surface and extends to lower crustal depths (8 s

TWT; ~20 km) (Figure 4, 5). Individual reflections are remarkably continuous within the package, continuing down-dip across depth intervals of >2.5 s TWT (Figure 4). The width of the reflection package increases at shallower depths, from ~2 km wide at 6-7 s TWT (~15 km), to ~5 km wide at 2-3 s TWT (~2.7 km) (Figure 4, 5). A reflection corresponding to the lower boundary of this package can be traced to the top Acoustic Basement surface, where the package delineates a 5-7 km wide subcrop at the top Acoustic Basement surface (Figure 4). A series of faults in the hanging wall of the Terrane Boundary Fault merge with said fault downdip, defining a series of fault blocks, with those at greater depths showing larger offset than those at shallow depths (Figure 4). The timing of activity along these hanging wall faults appears to occur later updip along the Terrane Boundary Fault, with deeper faults showing earlier activity than those at shallow depths (Figure 4). High amplitude reflections are present in the sedimentary sequence in the hangingwall of the Terrane Boundary Fault, and are likely related to coal intervals within the Upper Cretaceous Hoiho Group (Figure 4) (Killops et al. 1997).

In addition to the fault-parallel reflection package associated with the Terrane Boundary Fault, we observe further high-amplitude basement reflectivity at mid-crustal depths (4-6 s TWT; 6-12 km) in the footwall of the Terrane Boundary Fault, corresponding to Median Batholith Zone basement (Figure 4, 5). These reflection packages are typically sub-horizontal, although they dip slightly northwards further to the north. The reflection packages define areas of high- and low-reflectivity within crystalline basement. In the west, beneath the basin margin, the reflection packages extend from 3-6 s TWT (3.5-12.5 km) and reach close to the top basement surface (Figure 4). Beneath the basin further to the east, the packages do not extend to as shallow depths and are present from 5-7 s TWT (9-16.5 km) (Figure 5).

Based on its geometry and seismic reflection character, we interpret the fault-parallel reflection package in the footwall of the Terrane Boundary Fault as the seismic expression of a crustal-scale shear zone (here termed the Terrane Boundary Shear Zone). The reflection package resembles the characteristic seismic expression of shear zones, which arises through constructive interference between highly strained mylonite zones and intervening relatively undeformed material (Jones & Nur

1984; Carreras 2001; Reeve et al. 2013; Rennie et al. 2013; Phillips et al. 2016). Elsewhere, similar reflection packages have been confidently linked to onshore shear zones (Freeman et al. 1988; Wang et al. 1989; Fossen & Hurich 2005; Bird et al. 2014; Phillips et al. 2016; Fazlikhani et al. 2017; Lenhart et al. 2019) or those encountered in boreholes (Hedin et al. 2016).

We suggest the sub-horizontal reflection packages in the footwall of the Terrane Boundary Shear Zone represent a series of stacked igneous laccoliths. Granitic rocks are abundant across the Median Batholith Zone in this area (Mortimer et al. 1999; Tulloch et al. 2019), as indicated by granitic basement penetrated nearby boreholes (Figure 2) and exposed onshore Stewart Island (Figure 1). Basement penetrated by the Pukaki-1 well is correlated to the Separation Point Batholith Suite, which occupies a similar location along the southern margin of the Median Batholith to the structures interpreted here (Figure 5) (Allibone & Tulloch 2004; Tulloch et al. 2019). Similarly, the Pakaha-1 borehole penetrates granitic basement belonging to a Carboniferous-aged batholith suite (Figure 1) (Tulloch et al. 2019).

In addition, the reflection patterns identified here, of stacked sub-horizontal packages of high- and low-amplitude reflectivity, resemble those observed from the Lake District Batholith, where prominent reflections are generated between stacked granite laccolith sheets (Figure 4) (Evans et al. 1993; Evans et al. 1994). The interpreted lenticular geometries of the reflection packages here are also consistent with those expected from granitic laccoliths (McCaffrey & Petford 1997; Petford et al. 2000). Based on the regional distribution and dominantly granitic nature of basement rocks in this area, we prefer an igneous origin for these packages of reflectivity rather than one related to metamorphic basement lithologies (Lenhart et al. 2019). Although we have no direct constrains on the lithology of these reflection packages, based on their geometry and seismic character, in conjunction with the regional setting and nature of crystalline basement in this area, we interpret the reflection packages to represent a series of stacked, likely granitic, laccoliths.

As well as the shear zone and granite-related reflectivity in the footwall of the Terrane Boundary Fault, two seismic fabrics within basement are also pervasive throughout the area (Figure 4, 5). These fabrics are characterised by widespread relatively linear reflections and are often truncated at a high angle by the top Acoustic Basement surface. They fabrics often appear to display mutually cross-cutting relationships in cross-section, and are often associated with low-displacement faults at the top Acoustic Basement surface (Figure 4, 5).

5 Detailed rift geometry – 3D seismic volume

Two horizons mapped through the 3D seismic volume provide additional detail on fault geometries and rift physiography in the footwall of the Terrane Boundary Fault (Figure 6).

A WNW-trending structural high is present in the immediate footwall of the Terrane Boundary Fault, which we henceforth refer to as the Terrane Boundary Fault (TBF) Footwall Block (Figure 6a). The Terrane Boundary Fault is not clearly expressed at the Intra-upper Cretaceous structural level; although some minor, WNW-trending and SSW-dipping faults are present along the southern margin of the TBF Footwall Block (Figure 6b). The TBF Footwall Block is underpinned by the interpreted granitic laccoliths and may link with the Pakaha ridge to the east (Figure 1). Only a few, low-displacement WNW- and NE-trending faults are present across the TBF Footwall Block (Figure 6a). The northern margin of the TBF Footwall Block is largely parallel to the Terrane Boundary Fault, whilst a series of embayments are present along its southern margin (Figure 6a, 7). These embayments are 5-8 km wide, ~0.5 s TWT deep and incise about ~6 km back into the TBF Footwall Block (Figure 7).

A NE-trending fault is expressed at both the Acoustic Basement and intra-Upper Cretaceous surfaces to the northeast of the area (Figure 6). This fault forms a single structure in the northeast that splays into series of smaller segments to the southwest and is hereby referred to as the ‘Splaying Fault System’. Individual segments of the Splaying Fault System dip southeast and northwest, resulting in complex plan-view geometries across the Acoustic Basement and Intra-upper Cretaceous surfaces, and often non-resolvable relationships at depth (Figure 3, 6). Some NE-striking, SE-dipping faults are present in the southwest of the area, defining NE-trending structural highs superimposed onto the TBF Footwall Block (Figure 6). Reflectivity associated with the Splaying Fault System cross-cuts reflectivity in the footwall of the Terrane Boundary Fault, indicating that the Splaying Fault System formed after the Terrane Boundary Shear Zone and granitic material (Figure 6, 7).

5.1 Geometry and kinematics of the Splaying Fault System

By measuring throw across individual fault segments within the Splaying Fault System at both the Acoustic Basement and Intra-Upper Cretaceous structural levels, we are able to quantitatively analyse how strain is accommodated along the fault system (Figure 8, 9). Individual fault segments are better resolved across the Intra-Upper Cretaceous surface, meaning that they may provide a more complete record of strain distribution along the fault system, although not all faults offset this surface (Figure 9b).

In the northeast of the area the Splaying Fault System is represented by a single fault (Figure 8a), which accommodates ~800 ms (~1.8 km) and ~250 ms (~200 m) throw across the Acoustic Basement and Intra-Upper Cretaceous surfaces respectively (Figure 9). Two throw minima are present along the profile of this single fault plane (Fault 1), corresponding to bends in the fault trace formed by breached relay ramps along the fault (Fault 1; Figure 9). Sub-horizontal layered reflectivity beneath the Acoustic Basement surface in this area is interpreted as originating from sedimentary bedding, with some cross-cutting reflections interpreted as faults (Figure 8a). Any pre-Acoustic Basement strata is likely to be Jurassic to Early Cretaceous in age, potentially relating to earlier rift phases in the basin's formation (Uruski et al. 2007; Uruski 2010).

To the southwest, the Splaying Fault System begins to segment into a series of SE- and NW-dipping faults synthetic and antithetic to the main fault (Fault 1) respectively (Figure 6b, 8b). Fault segmentation is initially accommodated by dissection of the footwall into four fault segments that form a single plane at depth, and by the formation of antithetic hangingwall faults that appear to abut against the main fault structure at depth (Figure 8b). Additional NW-dipping faults in the footwall dip away from the main fault and further bisect the footwall (Figure 8b). This segmentation is accompanied by a decrease in throw along the main fault, as extension is accommodated by smaller fault segments in the footwall and hangingwall, with each segment accommodating 100-200 ms throw

(~200 m) at the Acoustic Basement surface (Figure 9a) and ~40 ms TWT at the Intra-Upper Cretaceous (Figure 9b). A key observation is that as the fault begins to splay, the cumulative throw across the whole system remains relatively constant. A slight minimum in the cumulative throw profile is present at ~24 km at the Acoustic Basement structural level (Figure 9a). However, as such a minimum is not observed at the Intra-Upper Cretaceous surface (Figure 9b), this may be related to a lack of imaging of faults in this area rather than a property of the system itself.

As the fault begins to splays at the intra-Upper Cretaceous surface, a new fault (F2; Figure 9b) forms in the hangingwall of Fault 1 and initially accommodates around ~150 ms (~200 m) throw compared to 25-50 ms (~50 m) throw across Fault 1 in the same location. In the northeast, Fault 1 appears to have been associated with a period of fault propagation folding prior to the brittle offset of the intra-upper Cretaceous surface, which is incorporated into the throw measurements for Fault 1 (Figure 8a). Therefore, when F2 forms in the hangingwall of Fault 1, the ductile deformation is incorporated into the throw measurements of F2 rather than Fault 1, which is now located in the footwall of F2 (Figure 9b).

Further southwest along the Splaying Fault System the footwall becomes highly deformed by both SE- and NW-dipping faults such that no dominant fault or overall hangingwall and footwall can be identified (Figure 8c). Here, extension is accommodated by multiple fault segments across a ~15 km wide zone (Figure 8c). Pre-acoustic basement sedimentary strata are again present in this area, although no divergent stratal wedges are identified in the hangingwalls of fault segments, indicating a lack of activity at that time (Figure 8c). Closer to the TBF Footwall Block the dominant fault appears to switch polarity, with a NW-dipping fault cross-cutting the SE-dipping fault that is dominant along-strike to the northeast (Figure 8d). Along the WNW-trending northern margin of the TBF Footwall Block segments of the Splaying Fault System begin to rotate around vertical axes to a WNW-striking orientation, dipping northeast, with horsetail splay geometries also identified across the Intra-Upper Cretaceous surface in some locations (Figure 6b). The rotation of individual fault segments in this area appears to be at least partially accommodated by their upwards splaying and bifurcation (Figure 8d). Individual fault segments tend to rotate and terminate along the northern margin of the TBF

Footwall Block, although some minor low-displacement faults (~20 ms TWT throw at the intra-Upper Cretaceous surface; Figure 10) continue further southwest (Figure 6, 9).

A series of NW-dipping faults to the east of the Splaying Fault System merge into a package of reflectivity at depth and join with an additional fault to the east that forms the border to a basement ridge (Figure 6, 8d). The geometry and structural style of these faults resemble those along the western border of the Pakaha ridge, where multiple faults root onto the margin of a granitic basement ridge (Figure 3, 8d).

6 Styles of structural inheritance

Having described and interpreted multiple structural heterogeneities located beneath the study area, we now document a number of different styles of interaction between these pre-existing structures and the later-formed rift-related faults. We examine how these structures are expressed within the rift system and how they influenced different aspects of the overall rift physiography.

6.1 Terrane boundary reactivation

The boundary between the Median Batholith and Western Province terranes in the study area is characterised by a major crustal-scale shear zone and associated upper-crustal fault system, the Terrane Boundary Shear Zone and Terrane Boundary Fault, as well as a series of granitic laccoliths that underpin the TBF Footwall Block. Regional seismic data indicates that the boundaries between individual terranes extend throughout the crust, and likely the lithosphere (Muir et al. 2000; Mortimer et al. 2002).

In the study area, the boundary between the Western Province terranes and the Median Batholith appears to have been exploited by the intrusion of the granitic laccoliths that underpin the TBF Footwall Block. In the North Island, the boundary between Median Batholith and Western Province terranes beneath the Taranaki Basin was exploited by the intrusion of Separation Point Batholith suite

(Muir et al. 2000; Collanega et al. 2018). This batholith suite is of similar affinity to the granitic basement sampled by the Pukaki-1 well along-strike of the terrane boundary in this location (Tulloch et al. 2019).

The Terrane Boundary Shear Zone localised along the margin of the granitic laccoliths, between the Median Batholith Zone and the Western Province terranes. This shear zone was then reactivated, forming the brittle Terrane Boundary Fault, during Late Cretaceous rifting associated with the breakup of Gondwana (Kula et al. 2007). This fault is associated with a series of fault blocks in its hangingwall and multiple embayments that incise into the footwall (Figure 4, 5, 7). Similarly in the North Island, the boundary between the Median Batholith and Western Province terranes was also reactivated, forming the Cape Egmont Fault Zone (Muir et al. 2000; Collanega et al. 2018).

The boundary between the Median Batholith and Western Province terranes in this area represents a crustal-scale structure that has localised strain and been repeatedly exploited and reactivated throughout its history. We suggest that differential stresses arising from the prominent rheological and lithological contrasts between the dominantly plutonic Median Batholith, , and the dominantly sedimentary Western Province terranes created a crustal-scale weakness that localised strain during subsequent tectonic events, leading to the repeated reactivation of the terrane boundary.

6.2 Strong crustal blocks as barriers to fault propagation

The Splaying Fault System splays towards the southwest before individual segments rotate and eventually terminate at the northern boundary of the TBF Footwall Block (Figure 6). As the fault segments and throw across any individual fault segment decreases, the cumulative throw remains relatively constant (Figure 9). A large throw gradient is present at the southwestern termination of the Splaying Fault System at both Acoustic Basement and Intra-Upper Cretaceous structural levels, at the northern margin of the TBF Footwall Block. Cumulative throw across the system decreases from ~150 ms to ~50 ms over a distance of 1-2 km at the Acoustic Basement surface, and it decreases from ~150 ms to ~50 ms over a similar distance at the intra-Upper Cretaceous surface. (Figure 9).

The relatively constant cumulative throw along the system suggests that the amount of extension accommodated by the fault is constant along its length. We propose that the TBF Footwall Block, underpinned by granitic material, represents an area of strong, relatively homogeneous crust, causing it to inhibit fault nucleation and act as a barrier to the lateral propagation of faults into the block from adjacent, relatively weaker crustal material.

Complex fault geometries occur at the southwestern termination of the Splaying Fault System along the northern margin of the TBF Footwall Block (Figure 10). Horsetail splay style geometries are situated at the terminations of Faults 15 and 16 across the Intra-Upper Cretaceous surface (Figure 10) (e.g. McGrath & Davison 1995; Kim et al. 2004). In these locations, NE-trending faults rotate sharply to NW and S/SE orientations at the boundary of the TBF Footwall Block, whilst also splaying into a series of segments that define small-scale graben structures (Figure 10). The graben structures are oriented parallel to the northern margin of the TBF Footwall Block and seemingly parallel to the regional NW-SE oriented extension direction (Figure 10). The grabens are only expressed across the Intra-upper Cretaceous surface. We suggest that these graben form as a consequence of the fault trying to reduce throw and terminate, in the presence of the stronger TBF Footwall Block to the southwest. Local stress perturbations proximal to the WNW-ESE oriented margin of the granitic TBF Footwall Block may have influenced the nearby faults, causing them to rotate to a more WNW-ESE orientation (Figure 10) (cf. Morley 2010; Rotevatn et al. 2018b; Samsu et al. 2019). Some NE-trending faults are identified to the south west of the horsetail splay faults (i.e. Faults 17 and 20 in Figure 10), forming E-W to NE-SW trending grabens within the TBF Footwall Block (Figure 4). We suggest that these relatively low-displacement faults broke through the initial barrier to propagation following an initial period of retardation at the northern margin of the TBF Footwall Block (Figure 10).

This stronger unit of crustal material appears more resistant to faulting than adjacent areas. As faults in these relatively weak adjacent areas propagate towards this stronger area, they begin to splay and segment, before eventually rotating and aligning along the actual boundary between the two units.

6.3 Reactivation of basement fabrics

Two prominent seismic fabrics are identified in crystalline basement across the study area, dipping towards the south (Figure 11) and to the east (Figure 12). These basement fabrics are most pronounced across the TBF Footwall Block, where they are shown to be associated with an E-W trending and a NE-SW trending fault population across the Acoustic Basement surface (Figure 6a). The different fabrics appear to display mutually cross-cutting relationships, with no interactions providing conclusive evidence for the relative timing of their formation (Figure 4, 5).

The E-W fabric aligns with and shares a similar S-dipping geometry as the Terrane Boundary Fault and shear zone. This fabric does not appear to be related to the NE-trending faults within the basin, including the Splaying Fault system, which cross-cut the fabric (Figure 11). The NE-SW fabric is aligned with, and displays a similar dip to, the NE-trending fault population. In cross-section, we observe that the fabrics associated with the NE-trending faults offset the E-W striking fabrics associated with the shear zone (Figure 7), indicating that the NE-SW fabric postdates the E-W fabric.

Prominent fabrics on seismic reflection data may be related to a number of different features including sedimentary strata, fault plane reflections, highly foliated basement rocks and shear zones (e.g. Phillips et al. 2016; Fazlikhani et al. 2017; Lenhart et al. 2019), and dyke swarms (e.g. Abdelmalak et al. 2015; Phillips et al. 2017). The E-W fabric appears related to the Terrane Boundary Fault and shear zone, appearing to link with the structure to the south (Figure 11). We suggest this basement fabric may represent a continuation of the TBF shear zone-related fabric through the TBF Footwall Block. The fabric in this location is exploited by multiple low-displacement faults (Figure 11). The generation of this fabric may relate to the initial phase of rift activity in the Great South Basin, related to the Late Cretaceous separation of Zealandia and Australia (Kula et al. 2007; Tulloch et al. 2019).

The NE-SW fabric appears to be related to the NE-trending faults that characterise the Great South Basin (Figure 1, 12). These faults formed due to NW-SE oriented extension between Zealandia and Western Antarctica (Kula et al. 2007; Sahoo et al. 2014; Tulloch et al. 2019), and faults associated with this extension are proposed to be listric and link to a detachment at mid-crustal depths (Uruski et al. 2007). The NE-SW fabric may possibly relate to this NW-SE oriented extension. Flexure in the hangingwalls of the larger, listric faults may have led to the reactivation of the fabric, which now hosts distributed minor faults (Figure 12).

7 Discussion

7.1 The regional evolution of the Great South Basin

The WNW-trending Terrane Boundary Fault is oriented at a high angle to the NE-trending faults of the Great South Basin (Figure 1). Whilst it is possible that local stress perturbations relating to pre-existing structures led to the development of non-optimally oriented structures such as the TBF (e.g. Morley 2010; Philippon et al. 2015; Phillips et al. 2016; Rotevatn et al. 2018b; Samsu et al. 2019), we do not think that this is the case due to the sub-perpendicular geometric relationship between the Terrane Boundary Fault and other NE-trending faults. Based on geometric relationships between the NE- and E-trending basement fabrics (Figure 7, 13c), we suggest that the WNW-trending structures formed prior to the NE-trending faults and fabrics. We propose that these non-collinear structures formed during multiple phases of extension relating to the multiphase breakup of Gondwana in the Late Cretaceous. An initial phase of extension occurred at 100-90 Ma, related to the breakup between Australia and the contiguous Zealandia and Western Antarctica. Offshore of the southeast South Island, the extension direction was oriented roughly NE-SW, perpendicular to the orientation of the basement terranes (Tulloch et al. 2019). The boundaries between basement terranes represented crustal-scale weaknesses that were optimally oriented tobe reactivated during this rift phase. We suggest that this initial phase of extension reactivated the boundary between the Median Batholith and Western Province terranes, forming the Terrane Boundary Shear Zone and Terrane Boundary Fault.

The Terrane Boundary Shear Zone is aligned with the Gutter Shear zone and the Freshwater and Escarpment fault systems within the Median Batholith Zone, which show dextral transpressional activity during the Early Cretaceous (Allibone & Tulloch 2004, 2008). While some oblique slip is possible along the Terrane Boundary Fault, we do not believe this to be the case based on the orientation of the embayments and the southwards dipping fault blocks within (Figure 6, 7). We suggest that the geometry of the Terrane Boundary Shear zone was primarily controlled by the boundary of the granitic laccoliths

Following breakup between Australia and Zealandia, a second phase of rifting occurred from ~90-80 Ma related to the breakup of Zealandia and Western Antarctica, leaving Zealandia as an isolated continent. The NE- to ENE-trending Sisters Shear Zone along the southern coast of Stewart Island is aligned with the northern margin of the Great South Basin and records extensional activity at this time (Kula et al. 2009). The NW-SE extension direction during this rift phase resulted in the formation of NE-trending faults across the Great South Basin (Beggs 1993; Uruski et al. 2007; Grobys et al. 2009; Sahoo et al. 2014). As the extension direction was oriented at a high angle to the WNW-trending Terrane boundary, this structure does not appear to have been active during this rift phase. However, the presence of the Terrane boundary Shear Zone, and the granitic laccoliths beneath the TBF Footwall Block, blocked the lateral propagation of faults forming at this time and acted to segment the overall rift (Figure 13b) (Dore et al. 1997; Corti 2008; Koopmann et al. 2014; Henstra et al. 2015; Peace et al. 2017; Heilman et al. 2019).

7.2 3D geometry and seismic expression of a granitic batholith

Although the Median Batholith represents a large area of igneous material, it is by no means a homogeneous body. The batholith is a composite structure formed during a protracted period of magmatism and comprises multiple generations of plutonic material with complex overprinting relationships as observed onshore (Mortimer et al. 1999; Allibone & Tulloch 2004). The Median Batholith as a whole represents a strong crustal unit relative to adjacent terranes. However, individual plutons within the composite structure, such as the granitic laccoliths interpreted here as part of the Separation Point Batholith suite, may represent relatively young, undeformed and therefore strong crustal units relative to adjacent older batholith suites which may have experienced more deformation and therefore may contain more heterogeneities upon which strain may localise. The large, composite nature of the Median Batholith resembles other batholiths worldwide, such as the Cordillera Blanca batholith of the Peruvian Andes (Petford & Atherton 1992) and the North American Sierra Nevada Batholith (Schwartz et al. 2014).

We suggest the granitic body underpinning the TBF Footwall Block belongs to the Cretaceous-aged Separation Point Batholith Suite. Intrusions displaying Separation Point affinity have been identified along the same terrane boundary in the Taranaki Basin (Mortimer et al. 1997; Muir et al. 2000), and form the basement of the Pukaki-1 well, which is also situated along the footwall of the Terrane Boundary Fault (Figure 1) (Tulloch et al. 2019). Late Early Cretaceous batholiths along-strike to the northwest on Stewart Island are largely confined to the south of the Gutter Shear zone, towards the boundary with the Western Province terranes (Mortimer et al. 1999; Allibone & Tulloch 2004). The Separation Point suite was intruded into Carboniferous-aged plutons, such as those penetrated in the Pakaha-1 well (Figure 1) (Tulloch et al. 2019). The spatial relationships between the granitic bodies offshore resembles those observed onshore Stewart Island (Allibone & Tulloch 2004).

Due to their relatively homogeneous nature, granitic bodies do not generate prominent impedance contrasts and often appear acoustically transparent on seismic reflection data. However, reflections can be generated at contacts between the granitic body and surrounding country rock, giving us insights into the gross morphology of the granitic body. Seismic reflections have previously been identified originating from the top and base of granitic bodies (Lynn et al. 1981; McLean et al. 2017; Howell et al. 2019), as well as from internal fracture zones (Mair & Green 1981) and layered granitic laccoliths (Evans et al. 1993; Evans et al. 1994). When observed in seismic data, granitic intrusions typically display a laccolith-style geometry, consisting of stacked, lenticular bodies similar to those observed here (Figure 4, 5, 13a) (Lynn et al. 1981; Evans et al. 1994; McCaffrey & Petford 1997; Petford et al. 2000). Across the TBF Footwall Block we identify some areas displaying relatively acoustically transparent seismic facies, which may correspond to the interpreted granitic laccoliths (Figure 11, 12). These acoustically transparent areas are cross-cut by shear zone-related reflectivity in some areas, representing faults and fractures within the granitic body itself (Figure 11).

Granitic material is often found beneath basement structural highs, such as the Utsira High in the North Sea (Slagstad et al. 2011; Lundmark et al. 2013); the Alston Block in the UK (Critchley 1984; Howell et al. 2019) and the Sierra Nevada Batholith in the USA (Ducea & Saleeby 1996; Van Buer et al. 2009). Previous studies have proposed that the reduced density and increased rigidity of granite compared to adjacent basement rocks makes them less susceptible to rifting when exposed to extensional stresses (Bott et al. 1958; de Castro et al. 2007). Whilst this increased buoyancy plays an important role in the formation of granite-cored structural highs, isostatic forces relating to initial granite emplacement also play an important role (Howell et al. 2019). These granitic bodies show a partitioning of strain and deformation around their margins rather than internally. One potential mechanism for the lack of faulting across granite-cored structural highs may be the absence of prominent heterogeneities within these relatively homogeneous bodies upon which strain can initially localise (Mair & Green 1981; Howell et al. 2019).

The geometry of the interpreted granite body shows some variability along-strike and is not at a constant depth beneath the top Acoustic Basement surface. In the west, the body extends up to ~3 s TWT (Figure 4). In the east, it displays a more domal geometry that extends up to ~5 s TWT, and stops at greater depths beneath the Acoustic Basement (Figure 5). Relief on the top surface of granitic bodies has been identified in the Lake District and North Pennine batholiths onshore UK (Howell et al. 2019). We propose that the relief atop the granite and its depth beneath the top Acoustic Basement surface is expressed in the rift physiography, controlling the location of embayments along the footwall of the Terrane Boundary Fault (Figure 14). In areas where the granitic body extends to shallow depths beneath the top Acoustic Basement surface, we identify a steep shear zone with a series of fault blocks detaching along its margin (Figure 4, 14). However, where the granite sits at greater depths beneath the top Acoustic Basement surface, the upper part of the shear zone rotates to shallower dips across the top of the granite and incises backwards into the TBF Footwall Block, creating embayments that contain ‘perched’ fault blocks atop a sub-horizontal detachment (Figure 5, 14). This indicates that the shallow relatively unfaulted areas of the TBF Footwall Block represent areas where the granite reaches shallow depths within basement and that the overall physiography of the TBF Footwall Block may act as a proxy for that of the underlying granite (Figure 6a, 14). This relief across the top of the granitic body may explain why the Terrane Boundary Shear zone localised along its margin thins with depth (Figure 4, 5). At deeper levels the shear zone is pinned along the margin of the granite, whereas at shallower depths, where the granite may be situated at deeper levels, the shear zone is less confined.

7.3 Strain accommodation along a laterally inhibited fault system

The Splaying Fault System segments as it approaches the granitic TBF Footwall Block (Figure 6). Cumulative fault throw remains relatively constant across the system as it approaches the block, with a large displacement gradient present towards the boundary with the block itself (Figure 9). The relatively constant cumulative throw along the fault indicates a large degree of kinematic coherence within the system, with individual fault segments behaving as a singular system (Walsh & Watterson 1991; Walsh et al. 2002; Walsh et al. 2003; Childs et al. 2017; Jackson et al. 2017; Rotevatn et al. 2018a). In cross-section, some faults also appear linked at depth, forming a single structure indicative of some degree of geometric coherence (Figure 8) (Walsh & Watterson 1991; Walsh et al. 2003; Giba et al. 2012; Jackson et al. 2017). However, whilst the NW-dipping fault segments splaying from the footwall block of the main structure display kinematic coherence with the main system they are not geometrically linked (Figure 8).

Although a steep gradient is present for cumulative throw on the Splaying Fault System at the boundary with the TBF Footwall Block, such a gradient is not apparent for the individual segments themselves, which display more typical throw profiles (Figure 9) (Childs et al. 2017). As the Splaying Fault System approaches this mechanically strong barrier to lateral fault propagation, it splays into a series of lower displacement segments. These segments display lower throw gradients and are able to terminate easier than a single large structure (Figure 13b). Similar splaying fault geometries are present at fault terminations across all scales. Deformation along the Alpine Fault onshore New Zealand is accommodated by splays of the Marlborough fault system to the northwest, where the fault starts to interact with the Hikurangi subduction zone further east (Norris & Cooper 2001; Wannamaker et al. 2009). Similarly, the eastern branch of the East African Rift forms a series of rift segments in the south, termed the North Tanzania Divergence Zone, where strain is accommodated over a wider area as rifting propagates toward and eventually terminates in the cratonic lithosphere of the Tanzania Craton (Ebinger et al. 1997; Foster et al. 1997; Ring et al. 2005). At smaller scales, geometrically similar structures, such as horsetail splays and damage zones are commonly associated with the lateral terminations of fault systems (Kim & Sanderson 2006; Mouslopoulou et al. 2007; Perrin et al. 2016; Nicol et al. 2017).

A key question is whether the fault propagated towards the TBF Footwall Block or whether the fault reached close to its full length geologically instantaneously (i.e. following the constant length fault model) (Walsh et al. 2002; Childs et al. 2017; Nicol et al. 2017) but displayed different structural styles along its length. Furthermore, it is also unclear why the fault splayed at this particular location, outboard of the TBF Footwall Block, rather than at the boundary itself. Nixon et al. (2014) document a transition from localised to distributed extension within a kinematically coherent fault system in the Whakatane Graben, which they link to progressive strain localisation along the system. However, the segmentation in this instance occurs over a relatively short distance and does not resemble the gradual increase in segmentation and the area over which strain is accommodated observed in the Splaying Fault System (Figure 6, 13b). If the entire fault length did form geologically instantaneously, rather than propagate to the southwest, why the fault changed structural style in that specific location would still require an explanation, as the boundary with the TBF Footwall Block is located to the southwest of the initial splay point, with no major change in underlying structure at the point of initial splaying. Damage zones relating to granite emplacement may have locally altered lithological properties of basement rocks; however, this would only affect a limited area. In addition, local rotation and alignment of fault segments are only identified along the margin of the TBF Footwall Block (Figure 6, 10), and are not present where the fault begins to splay. Based on the gradational splaying of the fault system and the apparent lack of change in basement physiography at the initial site of segmentation, we suggest that the fault propagated towards the granitic block, although the timescale of this propagation is shorter than the temporal resolution provided by our seismic data.

As the faults rotate at the margin of the TBF Footwall Block, they appear to detach from the granite, as they do along the Pakaha Ridge (Figure 3, 8d). One implication of this is that the northern margin of the granitic body dips to the north. Based on the information outlined above we propose the following model for why the fault splays where it does. Surrounding the TBF Footwall Block, the dipping margin of the stronger granitic material restricts the maximum fault height, such that where the faults interact with the granite boundary at depth is located north of and offset from the boundary at the surface (Figure 13b). The initial site of fault splaying would therefore correspond to the area where the deeper levels of the fault start to interact with the granitic body. As the fault approaches, its maximum height is reduced, causing the fault to splay into multiple segments (Figure 13b). Although this model could potentially explain the Splaying Fault System, we are unable to determine this scenario in our data.

As previously stated, individual fault segments rotate along the margin of the TBF Footwall Block (Figure 10, 13b). This may be related to local stress perturbations along the margin of the block (Morley 2010; Philippon et al. 2015; Morley 2017; Rotevatn et al. 2018b), or alternatively to a change in structural style along the faults from dip- to strike-slip following a 90° change in orientation (Mouslopoulou et al. 2007). The horsetail splay geometries identified across the intra-Upper Cretaceous surface (Figure 10) describe two WNW-trending grabens, which would not appear to be compatible with strike-slip motion. The grabens are not present at the top Acoustic Basement horizon and the individual faults may link together at depth, indicating that they could be related to oblique activity on a deeper fault. However, in other areas faults align along the margin of the TBF Footwall Block and show no evidence of strike-slip activity (Figure 6b). The rooting of faults onto the granitic body underpinning the TBF Footwall Block may also explain the switch in polarity along the Splaying Fault System, from SE-dipping in the northeast, to NW-dipping further southwest. In the southwest, the NW-dipping faults appear to detach onto the granitic body at depth, preferentially exploiting this pre-existing heterogeneity (Figure 8d).

5. Conclusions

In this study, we have analysed the detailed structural evolution of the southern section of the Great South Basin and examined how it has been influenced by various structural heterogeneities relating to the underlying Median Batholith Zone. We have documented a range of styles of structural inheritance, which exert variable influences over rift physiography throughout multiple tectonic events. We find that:

- The offshore extension of the boundary between the Median Batholith Zone and Western Province terranes, trends WNW across the Great South Basin. This terrane boundary is associated with a crustal-to-lithospheric scale shear zone and a series of faults in the upper crust that segment the Great South Basin. The terrane boundary was initially exploited by the intrusion of igneous plutonic material, before being reactivated in response to NE-SW oriented extension related to the separation of Australia and New Zealand.
- We postulate a granitic body forms a structural high in the footwall of the reactivated terrane boundary. Based on seismic interpretation, regional context and nearby well information, we interpret that the granitic body displays a laccolith-style geometry and is part of the Cretaceous Separation Point Batholith suite. This batholith suite may have exploited the original lithosphere-scale terrane boundary along the southern margin of the Median Batholith and later appeared to localise the shear zone along its southern margin.
- We infer details of the 3D geometry of the granitic body from the overlying rift physiography. Where the body reaches shallow depths, it controls the shallow geometry of the Terrane Boundary shear zone, which tracks along the margin and is associated with hangingwall fault blocks; where the granitic body top sits at greater depths, the shear zone shallows atop the structure and forms shallow embayments that incise into the footwall. These features act as a proxy for the relief of the top of the granitic body.

- The granitic body underpinning the TBF Footwall Block acts as a barrier to the lateral propagation of NE-trending faults within the Median Batholith. These faults form a series of splays that eventually rotate into parallelism as they approach the mechanically strong granitic body, with relatively few faults present across the high itself. NE-trending faults formed in response to NW-SE directed extension related to the separation and breakup of New Zealand and West Antarctica.
- Individual segments within the splaying fault system display kinematic and geometric coherence along the fault system and accommodate similar values of extension along-strike. The initial site of splaying along the fault system is offset from the boundary of the granitic body, perhaps relating to a N-dipping margin.
- Two generations of seismic fabrics are developed within basement beneath the basin, trending E-W and NE-SW. These fabrics are proposed to be related to the reactivation of the terrane boundary and the NW-SE directed rifting respectively. They are exploited by numerous small, low-displacement faults, which are particularly well developed atop the basement high.

Acknowledgements

This work is funded by the Leverhulme Trust in the form of a Leverhulme Early Career Fellowship awarded to Phillips. We would like to thank New Zealand Petroleum and Minerals for making the seismic data used in this study publically available. Seismic reflection and well data used in this study are publically available online via the New Zealand Petroleum and Minerals Exploration Database (https://www.nzpam.govt.nz/maps-geoscience/exploration-database/). We would also like to thank Schlumberger for providing academic licences to the University of Durham for the use of Petrel software. We thank Haakon Fossen, Craig Magee and an anonymous reviewer for their constructive reviews that have helped improve this manuscript, as well as Taylor Schildgen for editorial handling.

Figure captions

Figure 1 **–** Map showing the top Acoustic Basement structure surface (in two way travel time – TWT) across the study area of the Great South Basin in relation to the underlying basement terranes. Terrane boundaries after Ghisetti (2010) and Mortimer et al. (2002). The locations of wells in the area are shown by grey filled circles, red lines indicate the locations of seismic sections referred to in this study, and the blue polygon shows the outline of the 3D seismic volume. Major depocentre-bounding faults are highlighted by white lines. NE-trending faults are present throughout the basin, with a large WNW-trending fault present along its southern margin. Inset – regional map of New Zealand showing basement terranes offset along the Alpine Fault. Also shown are the locations of the Great South and Canterbury basins offshore the South Island, as well as bathymetric features including the Campbell Plateau, Chatham Rise and Bounty Trough.

Figure 2 **–** A) Stratigraphic columns showing New Zealand and International units. Regional stratigraphic ages referred to in this study are shown in bold, with the location of the Intra-upper Cretaceous surface also marked. B) Seismic well tie to the Pukaki-1 borehole. Gamma Ray, Sonic and Density logs are shown along with the synthetic and observed seismic traces. The input wavelet used for the generation of the synthetic seismic and a seismic trace from the seabed are shown below. The ages of stratigraphic horizons interpreted in this study are defined and placed into the regional framework of Mortimer et al. (2014). TVD – True Vertical Depth; TWT – Two-way-travel time. See Figure 1 for well location.

Figure 3 **–** Uninterpreted and interpreted E-W oriented seismic section across the centre of the Great South Basin. See Figure 1 for location. Key stratigraphic horizons are linked to the Pakaha-1 well. The Acoustic Basement is shown by the red line. In the east, some NE-dipping faults merge along the margin of the granitic Pakaha ridge. A complex series of cross-cutting faults are present in the centre of the basin.

Figure 4 **–** Uninterpreted and interpreted N-S oriented seismic section across the western platform of the study area. See Figure 1 for location. The boundary between the Median Batholith and Western Province terranes is marked by the thick blue line and is associated with a shear zone and fault system, termed the Terrane Boundary Shear Zone and Fault respectively. Divergent syn-rift strata are marked by dark green wedges. A large shear zone is co-located with the boundary between the terranes.

***Figure 5* –** uninterpreted and interpreted N-S oriented seismic section across the centre of the study area. See Figure 1 for location. The boundary between the Median Batholith and Western Province terranes is marked by the thick blue line. A large area of complex faulting is present in the footwall of the Terrane Boundary Fault.

***Figure 6* –** A) TWT structure map of the top Acoustic Basement surface based on 3D seismic volume across the centre of the basin, see Figure 1 for location. The basin is dominated by NE-trending faults with the SSW-dipping Terrane Boundary Fault along the southern margin of the basin. A WNW-trending, relatively unfaulted structural high is located in the footwall of the Terrane Boundary Fault, termed the TBF Footwall Block. B) TWT structure map of a key surface within the Upper Cretaceous interval (see Figure 3). A SE-dipping fault, the Splaying Fault System, becomes segmented towards the southwest and forms a series of splays as it approaches the TBF Footwall Block.

***Figure 7* –** uninterpreted and interpreted SW-NE oriented seismic section across the TBF Footwall Block and a prominent footwall embayment. See Figure 4 for location. Basement reflectivity is shown associated with the Terrane Boundary Shear Zone, with additional reflectivity at deeper levels related to granitic laccoliths. These fabrics are cross-cut by fabrics associated with the NE-trending faults.

***Figure 8* –** Uninterpreted and interpreted seismic sections along-strike of the Splaying Fault System. See Figure 4 for locations. A) Section across the north-eastern extent of the Splaying Fault System, where strain is accommodated by a single fault. Sub-Acoustic Basement reflectivity is present, likely relating to an earlier phase of activity of undetermined age. B) Towards the southwest the fault begins to splay into a series of segments. Synthetic fault segments form in response to dissection of the footwall as antithetic faults form in the hangingwall and merge with the main fault plane. C) The footwall of the fault is now highly deformed with extension accommodated by a wide zone of deformation consisting of SE- and NW-dipping faults. D) Extension is accommodated by a wide zone

of deformation, with the dominant faults now dipping to the NW and detaching onto the margin of a granitic ridge. Rotation of the faults to a WNW-ESE strike is accommodated by the formation of shallow synthetic and antithetic faults in the footwall and hangingwall of the faults respectively.

Figure 9 – Throw-length profiles calculated across the Acoustic Basement (A) and Intra-Upper Cretaceous (B) surfaces for individual segments of the Splaying Fault System. Individual profiles are colour-coded to the faults on the surface to the right. Cumulative throw across the whole of the system, calculated by summing throw on individual segments across a lines perpendicular to the strike projection of the main fault, is shown by the black dashed lines. Note that the cumulative throw is relatively consistent across the system regardless of the degree of segmentation, before a steep displacement gradient towards the boundary of the TBF Footwall Block. Also shown are the locations of the sections shown in Figure 8.

Figure 10 – Uninterpreted TWT structure map and detailed interpretations of horsetail-splay style fault geometries across the Intra-Upper Cretaceous surface. See Figure 4b for location. Fault numbers refer to those in Figure 10. Inset – Two seismic sections across the area corresponding to the blue and purple lines on the figure.

Figure 11 – Uninterpreted and interpreted NNE-SSW oriented seismic sections across the TBF Footwall Block, highlighting the E-W oriented basement fabrics. See Figures 4 and 14 for location. Shear-zone related reflectivity is shown by the thick dashed black lines, whilst the basement fabrics are represented by the dark blue lines. NE-trending faults post-date and cross-cut the shear zone related reflectivity.

Figure 12 – Uninterpreted and interpreted E-W oriented seismic section across the TBF Footwall Block, highlighting the NE-trending basement fabric. See Figures and 14 for location. The basement fabric displays a similar dip to the NE-trending faults and is often associated with low-displacement faults across the top Acoustic Basement surface.

Figure 13 – Schematic cartoons showing the different styles of structural inheritance identified in the Great South Basin across different scales. A) Shear zone and associated fault localise along the

Terrane boundary and the margin of the continuation of the Separation Point Batholith Suite between the Median Batholith and Western Province. Inset shows the localisation of the shear zone along the granite margin. B) The stronger material in the footwall to the Terrane Boundary Fault forms a barrier to lateral fault propagation, causing faults to splay as they approach and strain to be accommodated across multiple low-displacement segments. Inset – The dipping boundary of the strong barrier restricts fault height away from the boundary at the surface, causing the initial site of fault splaying to be offset from the boundary at shallower depths. C) Exploitation of prominent basement fabrics by relatively low-displacement faults. Differently oriented fabrics may be exploited at different times and during different tectonic events, resulting in multiple generations of faults. Inset – Cross-sectional view showing the reactivation and cross-cutting relationships between different fabrics.

***Figure 14* –** Conceptual 3D model showing the relationship between the Terrane Boundary Shear Zone and the relief of the top of the granitic body. The shear zone localises along the margin of the granite body. Where the granitic body is situated at shallower depths the shear zone tracks along the margin and is associated with a series of detaching fault blocks; where the shear zone is situated at greater depths, it shallows atop the body and forms embayments that cut back into the footwall.

References

Abdelmalak, M.M., Andersen, T.B., Planke, S., Faleide, J.I., Corfu, F., Tegner, C., Shephard, G.E., Zastrozhnov, D*., et al.* 2015. The ocean-continent transition in the mid-Norwegian margin: Insight from seismic data and an onshore Caledonian field analogue. *Geology*, **43**, 1011-1014, http://doi.org/10.1130/G37086.1.

Allibone, A.H. & Tulloch, A.J. 2004. Geology of the plutonic basement rocks of Stewart Island, New Zealand. *New Zealand Journal of Geology and Geophysics*, **47**, 233-256, http://doi.org/10.1080/00288306.2004.9515051.

Allibone, A.H. & Tulloch, A.J. 2008. Early Cretaceous dextral transpressional deformation within the Median Batholith, Stewart Island, New Zealand. *New Zealand Journal of Geology and Geophysics*, **51**, 115-134, http://doi.org/10.1080/00288300809509854.

Bache, F., Sutherland, R., Stagpoole, V., Herzer, R., Collot, J. & Rouillard, P. 2012. Stratigraphy of the southern Norfolk Ridge and the Reinga Basin: A record of initiation of Tonga–Kermadec–Northland subduction in the southwest Pacific. *Earth and Planetary Science Letters*, **321-322**, 41-53, http://doi.org/https://doi.org/10.1016/j.epsl.2011.12.041.

Bache, F., Mortimer, N., Sutherland, R., Collot, J., Rouillard, P., Stagpoole, V. & Nicol, A. 2014. Seismic stratigraphic record of transition from Mesozoic subduction to continental breakup in the Zealandia sector of eastern Gondwana. *Gondwana Research*, **26**, 1060-1078, http://doi.org/https://doi.org/10.1016/j.gr.2013.08.012.

Beggs, J. 1993. Depositional and tectonic history of the Great South Basin. *South Pacific sedimentary basins. Sedimentary basins of the World*, **2**, 365-373.

Bird, P.C., Cartwright, J.A. & Davies, T.L. 2014. Basement reactivation in the development of rift basins: an example of reactivated Caledonide structures in the West Orkney Basin. *Journal of the Geological Society*, **172**, 77-85, http://doi.org/10.1144/jgs2013-098.

Bishop, D., Bradshaw, J. & Landis, C. 1985. Provisional terrane map of South Island, New Zealand.

Bott, M.H.P., Day, A.A. & Massonsmith, D. 1958. The Geological Interpretation of Gravity and Magnetic Surveys in Devon and Cornwall. *Philosophical Transactions of the Royal Society of London Series a-Mathematical and Physical Sciences*, **251**, 161-191, http://doi.org/10.1098/rsta.1958.0013.

Bradshaw, J.D. 1989. Cretaceous Geotectonic Patterns in the New-Zealand Region. *Tectonics*, **8**, 803-820, http://doi.org/10.1029/TC008i004p00803.

Campbell, H.J., Mortimer, N. & Turnbull, I.M. 2003. Murihiku Supergroup, New Zealand: Redefined. *Journal of the Royal Society of New Zealand*, **33**, 85-95, http://doi.org/10.1080/03014223.2003.9517722.

Carreras, J. 2001. Zooming on Northern Cap de Creus shear zones. *Journal of Structural Geology*, **23**, 1457-1486, http://doi.org/https://doi.org/10.1016/S0191-8141(01)00011-6.

Chattopadhyay, A. & Chakra, M. 2013. Influence of pre-existing pervasive fabrics on fault patterns during orthogonal and oblique rifting: An experimental approach. *Marine and Petroleum Geology*, **39**, 74-91, http://doi.org/http://dx.doi.org/10.1016/j.marpetgeo.2012.09.009.

Childs, C., Holdsworth, R.E., Jackson, C.A.L., Manzocchi, T., Walsh, J.J. & Yielding, G. 2017. Introduction to the geometry and growth of normal faults. *Geological Society, London, Special Publications*, **439**, 1, http://doi.org/10.1144/SP439.24.

Coleman, A.J., Jackson, C.A.L., Nikolinakou, M.A. & Duffy, O.B. 2018. How, where, and when do radial faults grow near salt diapirs? *Geology*, **46**, 655-658, http://doi.org/10.1130/G40338.1.

Collanega, L., Jackson, C.A.L., Bell, R.E., Coleman, A.J., Lenhart, A. & Breda, A. 2018. Normal fault growth influenced by basement fabrics: the importance of preferential nucleation from pre-existing structures. *Basin Research*, **0**, http://doi.org/10.1111/bre.12327.

Cooper, A.F., Barreiro, B.A., Kimbrough, D.L. & Mattinson, J.M. 1987. Lamprophyre dike intrusion and the age of the Alpine fault, New Zealand. *Geology*, **15**, 941-944, http://doi.org/10.1130/0091-7613(1987)15<941:LDIATA>2.0.CO;2.

Corti, G. 2008. Control of rift obliquity on the evolution and segmentation of the main Ethiopian rift. *Nature Geoscience*, **1**, 258, http://doi.org/10.1038/ngeo160

https://www.nature.com/articles/ngeo160#supplementary-information.

Critchley, M.F. 1984. Variscan tectonics of the Alston block, northern England. *Geological Society, London, Special Publications*, **14**, 139, http://doi.org/10.1144/GSL.SP.1984.014.01.14.

Daly, M.C., Chorowicz, J. & Fairhead, J.D. 1989. Rift basin evolution in Africa: the influence of reactivated steep basement shear zones. *Geological Society, London, Special Publications*, **44**, 309, http://doi.org/10.1144/GSL.SP.1989.044.01.17.

Davy, B., Hoernle, K. & Werner, R. 2008. Hikurangi Plateau: Crustal structure, rifted formation, and Gondwana subduction history. *Geochemistry, Geophysics, Geosystems*, **9**, http://doi.org/10.1029/2007GC001855.

Dawson, S.M., Laó-Dávila, D.A., Atekwana, E.A. & Abdelsalam, M.G. 2018. The influence of the Precambrian Mughese Shear Zone structures on strain accommodation in the northern Malawi Rift. *Tectonophysics*, **722**, 53-68, http://doi.org/https://doi.org/10.1016/j.tecto.2017.10.010.

de Castro, D.L., de Oliveira, D.C. & Gomes Castelo Branco, R.M. 2007. On the tectonics of the Neocomian Rio do Peixe Rift Basin, NE Brazil: Lessons from gravity, magnetics, and radiometric data. *Journal of South American Earth Sciences*, **24**, 184-202, http://doi.org/https://doi.org/10.1016/j.jsames.2007.04.001.

De Paola, N., Holdsworth, R.E. & McCaffrey, K.J.W. 2005. The influence of lithology and pre-existing structures on reservoir-scale faulting patterns in transtensional rift zones. *Journal of the Geological Society*, **162**, 471, http://doi.org/10.1144/0016-764904-043.

Dichiarante, A.M., Holdsworth, R.E., Dempsey, E.D., Selby, D., McCaffrey, K.J.W., Michie, U.M., Morgan, G. & Bonniface, J. 2016. New structural and Re–Os geochronological evidence constraining the age of faulting and associated mineralization in the Devonian Orcadian Basin, Scotland. *Journal of the Geological Society*, **173**, 457, http://doi.org/10.1144/jgs2015-118.

Dore, A.G., Lundin, E.R., Fichler, C. & Olesen, O. 1997. Patterns of basement structure and reactivation along the NE Atlantic margin. *Journal of the Geological Society*, **154**, 85-92, http://doi.org/DOI 10.1144/gsjgs.154.1.0085.

Ducea, M.N. & Saleeby, J.B. 1996. Buoyancy sources for a large, unrooted mountain range, the Sierra Nevada, California: Evidence from xenolith thermobarometry. *Journal of Geophysical Research-Solid Earth*, **101**, 8229-8244, http://doi.org/10.1029/95jb03452.

Duffy, O.B., Bell, R.E., Jackson, C.A.L., Gawthorpe, R.L. & Whipp, P.S. 2015. Fault growth and interactions in a multiphase rift fault network: Horda Platform, Norwegian North Sea. *Journal of Structural Geology*, **80**, 99-119, http://doi.org/http://dx.doi.org/10.1016/j.jsg.2015.08.015.

Ebinger, C., Djomani, Y.P., Mbede, E., Foster, A. & Dawson, J.B. 1997. Rifting Archaean lithosphere: the Eyasi-Manyara-Natron rifts, East Africa. *Journal of the Geological Society*, **154**, 947, http://doi.org/10.1144/gsjgs.154.6.0947.

Evans, D.J., Rowley, W.J., Chadwick, R.A. & Millward, D. 1993. Seismic reflections from within the Lake District batholith, Cumbria, northern England. *Journal of the Geological Society*, **150**, 1043, http://doi.org/10.1144/gsjgs.150.6.1043.

Evans, D.J., Rowley, W.J., Chadwick, R.A., Kimbell, G.S. & Millward, D. 1994. Seismic reflection data and the internal structure of the Lake District batholith, Cumbria, northern England. *Proceedings of the Yorkshire Geological and Polytechnic Society*, **50**, 11, http://doi.org/10.1144/pygs.50.1.11.

Fazlikhani, H., Fossen, H., Gawthorpe, R., Faleide, J.I. & Bell, R.E. 2017. Basement structure and its influence on the structural configuration of the northern North Sea rift. *Tectonics*, **36**, 1151-1177, http://doi.org/10.1002/2017tc004514.

Fossen, H. & Hurich, C.A. 2005. The Hardangerfjord Shear Zone in SW Norway and the North Sea: a large-scale low-angle shear zone in the Caledonian crust. *Journal of the Geological Society*, **162**, 675-687, http://doi.org/10.1144/0016-764904-136.

Fossen, H., Khani, H.F., Faleide, J.I., Ksienzyk, A.K. & Dunlap, W.J. 2016. Post-Caledonian extension in the West Norway–northern North Sea region: the role of structural inheritance. *Geological Society, London, Special Publications*, **439**, http://doi.org/https://doi.org/10.1144/SP439.6.

Foster, A., Ebinger, C., Mbede, E. & Rex, D. 1997. Tectonic development of the northern Tanzanian sector of the East African Rift System. *Journal of the Geological Society*, **154**, 689, http://doi.org/10.1144/gsjgs.154.4.0689.

Freeman, B., Klemperer, S.L. & Hobbs, R.W. 1988. The deep structure of northern England and the Iapetus Suture zone from BIRPS deep seismic reflection profiles. *Journal of the Geological Society*, **145**, 727, http://doi.org/10.1144/gsjgs.145.5.0727.

Ghisetti, F. 2010. Seismic interpretation, Propsects and Strucutral Analysis, Great South Basin. Ministry of Economic Development New Zealand Unpublished Petroleum Report PR4173.

Giba, M., Walsh, J.J. & Nicol, A. 2012. Segmentation and growth of an obliquely reactivated normal fault. *Journal of Structural Geology*, **39**, 253-267, http://doi.org/10.1016/j.jsg.2012.01.004.

Grobys, J.W.G., Gohl, K., Uenzelmann-Neben, G., Davy, B. & Barker, D. 2009. Extensional and magmatic nature of the Campbell Plateau and Great South Basin from deep crustal studies. *Tectonophysics*, **472**, 213-225, http://doi.org/https://doi.org/10.1016/j.tecto.2008.05.003.

Grobys, J.W.G., Gohl, K., Davy, B., Uenzelmann-Neben, G., Deen, T. & Barker, D. 2007. Is the Bounty Trough off eastern New Zealand an aborted rift? *Journal of Geophysical Research: Solid Earth*, **112**, http://doi.org/10.1029/2005JB004229.

Hedin, P., Almqvist, B., Berthet, T., Juhlin, C., Buske, S., Simon, H., Giese, R., Krauß, F.*, et al.* 2016. 3D reflection seismic imaging at the 2.5km deep COSC-1 scientific borehole, central Scandinavian Caledonides. *Tectonophysics*, **689**, 40-55, http://doi.org/https://doi.org/10.1016/j.tecto.2015.12.013.

Heilman, E., Kolawole, F., Atekwana, E.A. & Mayle, M. 2019. Controls of Basement Fabric on the Linkage of Rift Segments. *Tectonics*, **0**, http://doi.org/10.1029/2018TC005362.

Henstra, G.A., Rotevatn, A., Gawthorpe, R.L. & Ravnås, R. 2015. Evolution of a major segmented normal fault during multiphase rifting: The origin of plan-view zigzag geometry. *Journal of Structural Geology*, **74**, 45-63, http://doi.org/https://doi.org/10.1016/j.jsg.2015.02.005.

Heron, P.J., Peace, A.L., McCaffrey, K., Welford, J.K., Wilson, R., van Hunen, J. & Pysklywec, R.N. 2019. Segmentation of rifts through structural inheritance: Creation of the Davis Strait. *Tectonics*, **0**, http://doi.org/10.1029/2019TC005578.

Higgs, K.E., Browne, G.H. & Sahoo, T.R. 2019. Reservoir characterisation of syn-rift and post-rift sandstones in frontier basins: An example from the Cretaceous of Canterbury and Great South basins, New Zealand. *Marine and Petroleum Geology*, **101**, 1-29, http://doi.org/https://doi.org/10.1016/j.marpetgeo.2018.11.030.

Howell, D.G. 1980. Mesozoic accretion of exotic terranes along the New Zealand segment of Gondwanaland. *Geology*, **8**, 487-491, http://doi.org/10.1130/0091-7613(1980)8<487:MAOETA>2.0.CO;2.

Howell, L., Egan, S., Leslie, G. & Clarke, S. 2019. Structural and geodynamic modelling of the influence of granite bodies during lithospheric extension: Application to the Carboniferous basins of northern England. *Tectonophysics*, http://doi.org/https://doi.org/10.1016/j.tecto.2019.02.008.

Jackson, C.A.L., Bell, R.E., Rotevatn, A. & Tvedt, A.B.M. 2017. Techniques to determine the kinematics of synsedimentary normal faults and implications for fault growth models. *Geological Society, London, Special Publications*, **439**, SP439.422, http://doi.org/10.1144/SP439.22.

Johnston, M.R. 2019. Chapter 2 The path to understanding the central terranes of Zealandia. *Geological Society, London, Memoirs*, **49**, 15-30, http://doi.org/10.1144/m49.2.

Jones, T.D. & Nur, A. 1984. The nature of seismic reflections from deep crustal fault zones. *Journal of Geophysical Research: Solid Earth*, **89**, 3153-3171, http://doi.org/10.1029/JB089iB05p03153.

Jongens, R. 2006. Structure of the Buller and Takaka Terrane rocks adjacent to the Anatoki Fault, northwest Nelson, New Zealand. *New Zealand Journal of Geology and Geophysics*, **49**, 443-461, http://doi.org/10.1080/00288306.2006.9515180.

Killops, S.D., Cook, R.A., Sykes, R. & Boudou, J.P. 1997. Petroleum potential and oil-source correlation in the Great South and Canterbury Basins. *New Zealand Journal of Geology and Geophysics*, **40**, 405-423, http://doi.org/10.1080/00288306.1997.9514773.

Kim, Y.-S. & Sanderson, D.J. 2006. Structural similarity and variety at the tips in a wide range of strike–slip faults: a review. *Terra Nova*, **18**, 330-344, http://doi.org/10.1111/j.1365-3121.2006.00697.x.

Kim, Y.-S., Peacock, D.C.P. & Sanderson, D.J. 2004. Fault damage zones. *Journal of Structural Geology*, **26**, 503-517, http://doi.org/https://doi.org/10.1016/j.jsg.2003.08.002.

Kirkpatrick, J.D., Bezerra, F.H.R., Shipton, Z.K., Do Nascimento, A.F., Pytharouli, S.I., Lunn, R.J. & Soden, A.M. 2013. Scale-dependent influence of pre-existing basement shear zones on rift faulting: a case study from NE Brazil. *Journal of the Geological Society*, **170**, 237, http://doi.org/10.1144/jgs2012-043.

Koopmann, H., Brune, S., Franke, D. & Breuer, S. 2014. Linking rift propagation barriers to excess magmatism at volcanic rifted margins. *Geology*, **42**, 1071-1074, http://doi.org/10.1130/G36085.1.

Kula, J., Tulloch, A., Spell, T.L. & Wells, M.L. 2007. Two-stage rifting of Zealandia-Australia-Antarctica: Evidence from 40Ar/39Ar thermochronometry of the Sisters shear zone, Stewart Island, New Zealand. *Geology*, **35**, 411-414, http://doi.org/10.1130/g23432a.1.

Kula, J., Tulloch, A.J., Spell, T.L., Wells, M.L. & Zanetti, K.A. 2009. Thermal evolution of the Sisters shear zone, southern New Zealand; Formation of the Great South Basin and onset of Pacific-Antarctic spreading. *Tectonics*, **28**, http://doi.org/10.1029/2008TC002368.

Lamb, S., Mortimer, N., Smith, E. & Turner, G. 2016. Focusing of relative plate motion at a continental transform fault: Cenozoic dextral displacement >700 km on New Zealand's Alpine Fault, reversing >225 km of Late Cretaceous sinistral motion. *Geochemistry, Geophysics, Geosystems*, **17**, 1197-1213, http://doi.org/10.1002/2015GC006225.

Landis, C.A., Campbell, H.J., Aslund, T., Cawood, P.A., Douglas, A., Kimbrough, D.L., Pillai, D.D.L., Raine, J.I.*, et al.* 1999. Permian-Jurassic strata at Productus Creek, Southland, New Zealand:

Implications for terrane dynamics of the eastern Gondwanaland margin. *New Zealand Journal of Geology and Geophysics*, **42**, 255-278, http://doi.org/10.1080/00288306.1999.9514844.

Lenhart, A., Jackson, C.A.L., Bell, R.E., Duffy, O.B., Gawthorpe, R.L. & Fossen, H. 2019. Structural architecture and composition of crystalline basement offshore west Norway. http://doi.org/10.1130/L668.1.

Long, J.J. & Imber, J. 2012. Strain compatibility and fault linkage in relay zones on normal faults. *Journal of Structural Geology*, **36**, 16-26, http://doi.org/https://doi.org/10.1016/j.jsg.2011.12.013.

Lundmark, A.M., Saether, T. & Sorlie, R. 2013. Ordovician to Silurian magmatism on the Utsira High, North Sea: implications for correlations between the onshore and offshore Caledonides. *Geological Society, London, Special Publications*, **390**, 513-523, http://doi.org/10.1144/sp390.21.

Lynn, H.B., Hale, L.D. & Thompson, G.A. 1981. Seismic Reflections from the Basal Contacts of Batholiths. *Journal of Geophysical Research*, **86**, 633-638, http://doi.org/10.1029/JB086iB11p10633.

Magee, C., McDermott, K.G., Stevenson, C.T.E. & Jackson, C.A.L. 2014. Influence of crystallised igneous intrusions on fault nucleation and reactivation during continental extension. *Journal of Structural Geology*, **62**, 183-193, http://doi.org/https://doi.org/10.1016/j.jsg.2014.02.003.

Mair, J.A. & Green, A.G. 1981. High-resolution seismic reflection profiles reveal fracture zones within a ‘homogeneous’ granite batholith. *Nature*, **294**, 439-442, http://doi.org/10.1038/294439a0.

McCaffrey, K.J.W. & Petford, N. 1997. Are granitic intrusions scale invariant? *Journal of the Geological Society*, **154**, 1, http://doi.org/10.1144/gsjgs.154.1.0001.

McGrath, A.G. & Davison, I. 1995. Damage zone geometry around fault tips. *Journal of Structural Geology*, **17**, 1011-1024, http://doi.org/https://doi.org/10.1016/0191-8141(94)00116-H.

McLean, C.E., Schofield, N., Brown, D.J., Jolley, D.W. & Reid, A. 2017. 3D seismic imaging of the shallow plumbing system beneath the Ben Nevis Monogenetic Volcanic Field: Faroe–Shetland Basin. *Journal of the Geological Society*, **174**, 468, http://doi.org/10.1144/jgs2016-118.

McWilliams, M.O. & Howell, D.G. 1982. Exotic terranes of western California. *Nature*, **297**, 215-217, http://doi.org/10.1038/297215a0.

Morley, C.K. 2010. Stress re-orientation along zones of weak fabrics in rifts: An explanation for pure extension in ‘oblique’ rift segments? *Earth and Planetary Science Letters*, **297**, 667-673, http://doi.org/https://doi.org/10.1016/j.epsl.2010.07.022.

Morley, C.K. 2017. The impact of multiple extension events, stress rotation and inherited fabrics on normal fault geometries and evolution in the Cenozoic rift basins of Thailand. *Geological Society, London, Special Publications*, **439**, 413, http://doi.org/10.1144/SP439.3.

Morley, C.K., Haranya, C., Phoosongsee, W., Pongwapee, S., Kornsawan, A. & Wonganan, N. 2004. Activation of rift oblique and rift parallel pre-existing fabrics during extension and their effect on deformation style: examples from the rifts of Thailand. *Journal of Structural Geology*, **26**, 1803-1829, http://doi.org/https://doi.org/10.1016/j.jsg.2004.02.014.

Morley, C.K., Maczak, A., Rungprom, T., Ghosh, J., Cartwright, J.A., Bertoni, C. & Panpichityota, N. 2017. New style of honeycomb structures revealed on 3D seismic data indicate widespread diagenesis offshore Great South Basin, New Zealand. *Marine and Petroleum Geology*, **86**, 140-154, http://doi.org/10.1016/j.marpetgeo.2017.05.035.

Mortimer, E.J., Paton, D.A., Scholz, C.A. & Strecker, M.R. 2016. Implications of structural inheritance in oblique rift zones for basin compartmentalization: Nkhata Basin, Malawi Rift (EARS). *Marine and Petroleum Geology*, **72**, 110-121, http://doi.org/https://doi.org/10.1016/j.marpetgeo.2015.12.018.

Mortimer, N. 2004. New Zealand's Geological Foundations. *Gondwana Research*, **7**, 261-272, http://doi.org/https://doi.org/10.1016/S1342-937X(05)70324-5.

Mortimer, N. 2014. The oroclinal bend in the South Island, New Zealand. *Journal of Structural Geology*, **64**, 32-38, http://doi.org/https://doi.org/10.1016/j.jsg.2013.08.011.

Mortimer, N., Tulloch, A.J. & Ireland, T.R. 1997. Basement geology of Taranaki and Wanganui Basins, New Zealand. *New Zealand Journal of Geology and Geophysics*, **40**, 223-236, http://doi.org/10.1080/00288306.1997.9514754.

Mortimer, N., Davey, F.J., Melhuish, A., Yu, J. & Godfrey, N.J. 2002. Geological interpretation of a deep seismic reflection profile across the Eastern Province and Median Batholith, New Zealand: Crustal architecture of an extended Phanerozoic convergent orogen. *New Zealand Journal of Geology and Geophysics*, **45**, 349-363, http://doi.org/10.1080/00288306.2002.9514978.

Mortimer, N., Tulloch, A.J., Spark, R.N., Walker, N.W., Ladley, E., Allibone, A. & Kimbrough, D.L. 1999. Overview of the Median Batholith, New Zealand: a new interpretation of the geology of the Median Tectonic Zone and adjacent rocks. *Journal of African Earth Sciences*, **29**, 257-268, http://doi.org/https://doi.org/10.1016/S0899-5362(99)00095-0.

Mortimer, N., Rattenbury, M.S., King, P.R., Bland, K.J., Barrell, D.J.A., Bache, F., Begg, J.G., Campbell, H.J.*, et al.* 2014. High-level stratigraphic scheme for New Zealand rocks. *New Zealand Journal of Geology and Geophysics*, **57**, 402-419, http://doi.org/10.1080/00288306.2014.946062.

Mouslopoulou, V., Nicol, A., Little, T.A. & Walsh, J.J. 2007. Displacement transfer between intersecting regional strike-slip and extensional fault systems. *Journal of Structural Geology*, **29**, 100-116, http://doi.org/https://doi.org/10.1016/j.jsg.2006.08.002.

Muir, R.J., Bradshaw, J.D., Weaver, S.D. & Laird, M.G. 2000. The influence of basement structure on the evolution of the Taranaki Basin, New Zealand. *Journal of the Geological Society*, **157**, 1179, http://doi.org/10.1144/jgs.157.6.1179.

Nicol, A., Childs, C., Walsh, J.J., Manzocchi, T. & Schöpfer, M.P.J. 2017. Interactions and growth of faults in an outcrop-scale system. *Geological Society, London, Special Publications*, **439**, 23, http://doi.org/10.1144/SP439.9.

Nixon, C.W., Bull, J.M. & Sanderson, D.J. 2014. Localized vs distributed deformation associated with the linkage history of an active normal fault, Whakatane Graben, New Zealand. *Journal of Structural Geology*, **69**, 266-280, http://doi.org/https://doi.org/10.1016/j.jsg.2014.06.005.

Norris, R.J. & Cooper, A.F. 2001. Late Quaternary slip rates and slip partitioning on the Alpine Fault, New Zealand. *Journal of Structural Geology*, **23**, 507-520, http://doi.org/https://doi.org/10.1016/S0191-8141(00)00122-X.

Paton, D.A. & Underhill, J.R. 2004. Role of crustal anisotropy in modifying the structural and sedimentological evolution of extensional basins: the Gamtoos Basin, South Africa. *Basin Research*, **16**, 339-359, http://doi.org/10.1111/j.1365-2117.2004.00237.x.

Paton, D.A., Mortimer, E.J., Hodgson, N. & van der Spuy, D. 2016. The missing piece of the South Atlantic jigsaw: when continental break-up ignores crustal heterogeneity. *Geological Society, London, Special Publications*, **438**, SP438.438, http://doi.org/10.1144/SP438.8.

Peace, A., McCaffrey, K., Imber, J., van Hunen, J., Hobbs, R. & Wilson, R. 2017. The role of pre-existing structures during rifting, continental breakup and transform system development, offshore West Greenland. *Basin Research*, 373-394, http://doi.org/ https://doi.org/10.1111/bre.12257.

Perrin, C., Manighetti, I. & Gaudemer, Y. 2016. Off-fault tip splay networks: A genetic and generic property of faults indicative of their long-term propagation. *Comptes Rendus Geoscience*, **348**, 52-60, http://doi.org/https://doi.org/10.1016/j.crte.2015.05.002.

Petford, N. & Atherton, M.P. 1992. Granitoid emplacement and deformation along a major crustal lineament: The Cordillera Blanca, Peru. *Tectonophysics*, **205**, 171-185, http://doi.org/https://doi.org/10.1016/0040-1951(92)90425-6.

Petford, N., Cruden, A.R., McCaffrey, K.J.W. & Vigneresse, J.L. 2000. Granite magma formation, transport and emplacement in the Earth's crust. *Nature*, **408**, 669-673, http://doi.org/10.1038/35047000.

Philippon, M., Willingshofer, E., Sokoutis, D., Corti, G., Sani, F., Bonini, M. & Cloetingh, S. 2015. Slip re-orientation in oblique rifts. *Geology*, **43**, 147-150, http://doi.org/10.1130/G36208.1.

Phillips, T.B., Magee, C., Jackson, C.A.L. & Bell, R.E. 2017. Determining the three-dimensional geometry of a dike swarm and its impact on later rift geometry using seismic reflection data. *Geology*, **46**, 119-122, http://doi.org/10.1130/G39672.1.

Phillips, T.B., Jackson, C.A.L., Bell, R.E. & Duffy, O.B. 2018. Oblique reactivation of lithosphere-scale lineaments controls rift physiography – the upper-crustal expression of the Sorgenfrei–Tornquist Zone, offshore southern Norway. *Solid Earth*, **9**, 403-429, http://doi.org/10.5194/se-9-403-2018.

Phillips, T.B., Jackson, C.A., Bell, R.E., Duffy, O.B. & Fossen, H. 2016. Reactivation of intrabasement structures during rifting: A case study from offshore southern Norway. *Journal of Structural Geology*, **91**, 54-73, http://doi.org/10.1016/j.jsg.2016.08.008.

Reeve, M.T., Bell, R.E. & Jackson, C.A.L. 2013. Origin and significance of intra-basement seismic reflections offshore western Norway. *Journal of the Geological Society*, **171**, 1-4, http://doi.org/10.1144/jgs2013-020.

Rennie, S.F., Fagereng, Å. & Diener, J.F.A. 2013. Strain distribution within a km-scale, mid-crustal shear zone: The Kuckaus Mylonite Zone, Namibia. *Journal of Structural Geology*, **56**, 57-69, http://doi.org/https://doi.org/10.1016/j.jsg.2013.09.001.

Ring, U. 1994. The influence of preexisting structure on the evolution of the Cenozoic Malawi rift (East African rift system). *Tectonics*, **13**, 313-326, http://doi.org/10.1029/93TC03188.

Ring, U.W.E., Schwartz, H.L., Bromage, T.G. & Sanaane, C. 2005. Kinematic and sedimentological evolution of the Manyara Rift in northern Tanzania, East Africa. *Geological Magazine*, **142**, 355-368, http://doi.org/10.1017/S0016756805000841.

Roberts, A.M. & Holdsworth, R.E. 1999. Linking onshore and offshore structures: Mesozoic extension in the Scottish Highlands. *Journal of the Geological Society*, **156**, 1061, http://doi.org/10.1144/gsjgs.156.6.1061.

Robertson, A.H.F. & Palamakumbura, R. 2019. Chapter 9 Sedimentary development of the Mid-Permian–Mid-Triassic Maitai continental margin forearc basin, South Island, New Zealand. *Geological Society, London, Memoirs*, **49**, 189-230, http://doi.org/10.1144/m49.9.

Robertson, A.H.F., Campbell, H.J., Johnston, M.R. & Palamakumbra, R. 2019. Chapter 15 Construction of a Paleozoic–Mesozoic accretionary orogen along the active continental margin of SE Gondwana (South Island, New Zealand): summary and overview. *Geological Society, London, Memoirs*, **49**, 331-372, http://doi.org/10.1144/m49.8.

Rotevatn, A., Jackson, C.A.L., Tvedt, A.B.M., Bell, R.E. & Blækkan, I. 2018a. How do normal faults grow? *Journal of Structural Geology*, http://doi.org/https://doi.org/10.1016/j.jsg.2018.08.005.

Rotevatn, A., Kristensen, T.B., Ksienzyk, A.K., Wemmer, K., Henstra, G.A., Midtkandal, I., Grundvåg, S.-A. & Andresen, A. 2018b. Structural Inheritance and Rapid Rift-Length Establishment in a Multiphase Rift: The East Greenland Rift System and its Caledonian Orogenic Ancestry. *Tectonics*, **37**, 1858-1875, http://doi.org/doi:10.1029/2018TC005018.

Sahoo, T., King, P., Bland, K., Strogen, D., Sykes, R. & Bache, F. 2014. Tectono-sedimentary evolution and source rock distribution of the mid to Late Cretaceous succession in the Great South Basin, New Zealand *The APPEA Journal*, **54**, 259-274, http://doi.org/https://doi.org/10.1071/AJ13026.

Samsu, A., Cruden, A.R., Hall, M., Micklethwaite, S. & Denyszyn, S.W. 2019. The influence of basement faults on local extension directions: Insights from potential field geophysics and field observations. *Basin Research*, **0**, http://doi.org/10.1111/bre.12344.

Schwartz, J.J., Johnson, K., Mueller, P., Strickland, A., Valley, J. & Wooden, J.L. 2014. Time scales and processes of Cordilleran batholith construction and high-Sr/Y magmatic pulses: Evidence from the Bald Mountain batholith, northeastern Oregon. *Geosphere*, **10**, 1456-1481, http://doi.org/10.1130/GES01033.1.

Slagstad, T., Davidsen, B. & Daly, J.S. 2011. Age and composition of crystalline basement rocks on the Norwegian continental margin: offshore extension and continuity of the Caledonian–Appalachian orogenic belt. *Journal of the Geological Society*, **168**, 1167, http://doi.org/10.1144/0016-76492010-136.

Sutherland, R., Davey, F. & Beavan, J. 2000. Plate boundary deformation in South Island, New Zealand, is related to inherited lithospheric structure. *Earth and Planetary Science Letters*, **177**, 141-151, http://doi.org/https://doi.org/10.1016/S0012-821X(00)00043-1.

Sutherland, R., Collot, J., Lafoy, Y., Logan, G.A., Hackney, R., Stagpoole, V., Uruski, C., Hashimoto, T., *et al.* 2010. Lithosphere delamination with foundering of lower crust and mantle caused permanent subsidence of New Caledonia Trough and transient uplift of Lord Howe Rise during Eocene and Oligocene initiation of Tonga-Kermadec subduction, western Pacific. *Tectonics*, **29**, http://doi.org/10.1029/2009TC002476.

Thomas, W.A. 2006. Tectonic inheritance at a continental margin. *GSA Today*, **16**, 4-11, http://doi.org/10.1130/1052-5173(2006)016<4:TIAACM>2.0.CO;2.

Thomas, W.A. 2018. Tectonic inheritance at multiple scales during more than two complete Wilson cycles recorded in eastern North America. *Geological Society, London, Special Publications*, **470**, SP470.474, http://doi.org/10.1144/SP470.4.

Tommasi, A. & Vauchez, A. 2001. Continental rifting parallel to ancient collisional belts: an effect of the mechanical anisotropy of the lithospheric mantle. *Earth and Planetary Science Letters*, **185**, 199-210, http://doi.org/10.1016/S0012-821x(00)00350-2.

Tulloch, A., Mortimer, N., Ireland, T., Waight, T., Maas, R., Palin, M., Sahoo, T., Seebeck, H., *et al.* 2019. Reconnaissance basement geology and tectonics of South Zealandia. *Tectonics*, **0**, http://doi.org/10.1029/2018TC005116.

Tulloch, A.J. 1988. Batholiths, plutons, and suites: nomenclature for granitoid rocks of Westland—Nelson, New Zealand. *New Zealand Journal of Geology and Geophysics*, **31**, 505-509, http://doi.org/10.1080/00288306.1988.10422147.

Tulloch, A.J., Kimbrough, D.L., Landis, C.A., Mortimer, N. & Johnston, M.R. 1999. Relationships between the brook street Terrane and Median Tectonic Zone (Median Batholith): Evidence from Jurassic conglomerates. *New Zealand Journal of Geology and Geophysics*, **42**, 279-293, http://doi.org/10.1080/00288306.1999.9514845.

Tulloch, A.J., Ramezani, J., Kimbrough, D.L., Faure, K. & Allibone, A.H. 2009. U-Pb geochronology of mid-Paleozoic plutonism in western New Zealand: Implications for S-type granite generation and growth of the east Gondwana marginU-Pb geochronology of Paleozoic plutonism, New Zealand. *GSA Bulletin*, **121**, 1236-1261, http://doi.org/10.1130/B26272.1.

Uruski, C. 2015. The contribution of offshore seismic data to understanding the evolution of the New Zealand continent. *Sedimentary Basins and Crustal Processes at Continental Margins: From Modern Hyper-Extended Margins to Deformed Ancient Analogues*, **413**, 35-51, http://doi.org/10.1144/Sp413.1.

Uruski, C., Kennedy, C., Harrison, T., Maslen, G., Cook, R., Sutherland, R. & Zhu, H. 2007. Petroleum potential of the Great South Basin, New Zealand—New seismic data improves imaging. *The APPEA Journal*, **47**, 145-161, http://doi.org/https://doi.org/10.1071/AJ06008.

Uruski, C.I. 2010. New Zealand's deepwater frontier. *Marine and Petroleum Geology*, **27**, 2005-2026, http://doi.org/https://doi.org/10.1016/j.marpetgeo.2010.05.010.

Van Buer, N.J., Miller, E.L. & Dumitru, T.A. 2009. Early Tertiary paleogeologic map of the northern Sierra Nevada batholith and the northwestern Basin and Range. *Geology*, **37**, 371-374, http://doi.org/10.1130/g25448a.1.

Vasconcelos, D.L., Bezerra, F.H.R., Medeiros, W.E., de Castro, D.L., Clausen, O.R., Vital, H. & Oliveira, R.G. 2019. Basement fabric controls rift nucleation and postrift basin inversion in the continental margin of NE Brazil. *Tectonophysics*, **751**, 23-40, http://doi.org/https://doi.org/10.1016/j.tecto.2018.12.019.

Walsh, J.J. & Watterson, J. 1991. Geometric and kinematic coherence and scale effects in normal fault systems. *Geological Society, London, Special Publications*, **56**, 193-203, http://doi.org/https://doi.org/10.1144/GSL.SP.1991.056.01.13.

Walsh, J.J., Nicol, A. & Childs, C. 2002. An alternative model for the growth of faults. *Journal of Structural Geology*, **24**, 1669-1675, http://doi.org/https://doi.org/10.1016/S0191-8141(01)00165-1.

Walsh, J.J., Watterson, J., Childs, C. & Nicol, A. 1996. Ductile strain effects in the analysis of seismic interpretations of normal fault systems. *Geological Society, London, Special Publications*, **99**, 27, http://doi.org/10.1144/GSL.SP.1996.099.01.04.

Walsh, J.J., Bailey, W.R., Childs, C., Nicol, A. & Bonson, C.G. 2003. Formation of segmented normal faults: a 3-D perspective. *Journal of Structural Geology*, **25**, 1251-1262, http://doi.org/https://doi.org/10.1016/S0191-8141(02)00161-X.

Wang, C.-Y., Okaya, D.A., Ruppert, C., Davis, G.A., Guo, T.-S., Zhong, Z. & Wenk, H.-R. 1989. Seismic reflectivity of the Whipple Mountain shear zone in southern California. *Journal of Geophysical Research: Solid Earth*, **94**, 2989-3005, http://doi.org/10.1029/JB094iB03p02989.

Wannamaker, P.E., Caldwell, T.G., Jiracek, G.R., Maris, V., Hill, G.J., Ogawa, Y., Bibby, H.M., Bennie, S.L., *et al.* 2009. Fluid and deformation regime of an advancing subduction system at Marlborough, New Zealand. *Nature*, **460**, 733, http://doi.org/10.1038/nature08204

https://www.nature.com/articles/nature08204#supplementary-information.

Wellman, H.W. 1953. Data for the study of recent and late Pleistocene faulting in the South Island of New Zealand. *New Zealand Journal of Science and Technology*, **34 B**, 270-288.

Wenker, S. & Beaumont, C. 2016. Effects of lateral strength contrasts and inherited heterogeneities on necking and rifting of continents. *Tectonophysics*, http://doi.org/https://doi.org/10.1016/j.tecto.2016.10.011.

Whipp, P.S., Jackson, C.A.L., Gawthorpe, R.L., Dreyer, T. & Quinn, D. 2014. Normal fault array evolution above a reactivated rift fabric; a subsurface example from the northern Horda Platform, Norwegian North Sea. *Basin Research*, **26**, 523-549, http://doi.org/10.1111/bre.12050.

Wilson, J.T. 1966. Did the Atlantic Close and then Re-Open? *Nature*, **211**, 676-681, http://doi.org/10.1038/211676a0.

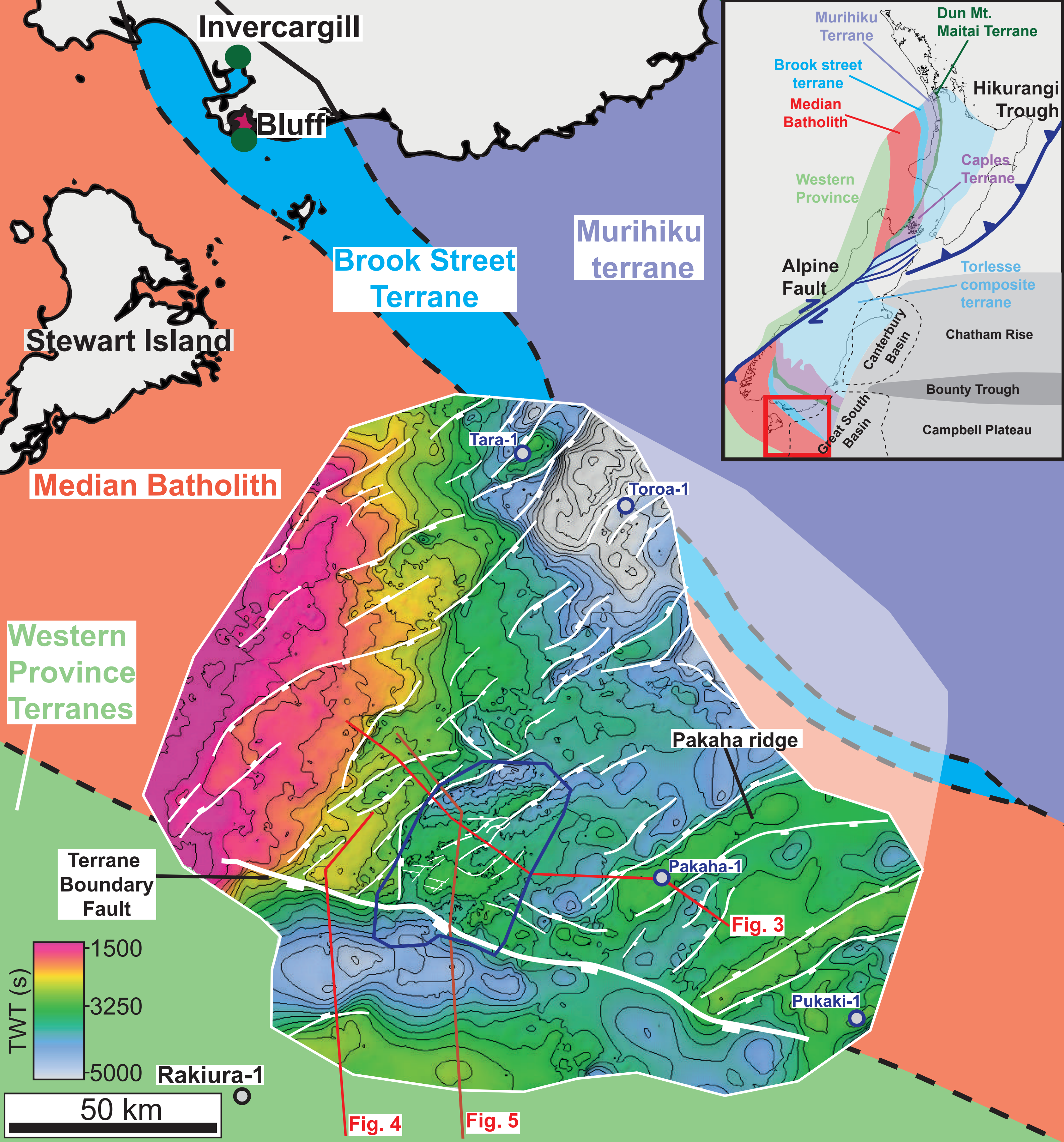
Invercargill
Bluff
Stewart Island
Brook Street Terrane
Murihiku terrane
Median Batholith
Western Province Terranes
Tara-1
Toroa-1
Pakaha ridge
Pakaha-1
Pukaki-1
Rakiura-1
Terrane Boundary Fault
Fig. 3
Fig. 4
Fig. 5
TWT (s)
1500
3250
5000
50 km
Murihiku Terrane
Dun Mt. Maitai Terrane
Brook street terrane
Median Batholith
Hikurangi Trough
Caples Terrane
Western Province
Alpine Fault
Torlesse composite terrane
Chatham Rise
Canterbury Basin
Bounty Trough
Great South Basin
Campbell Plateau

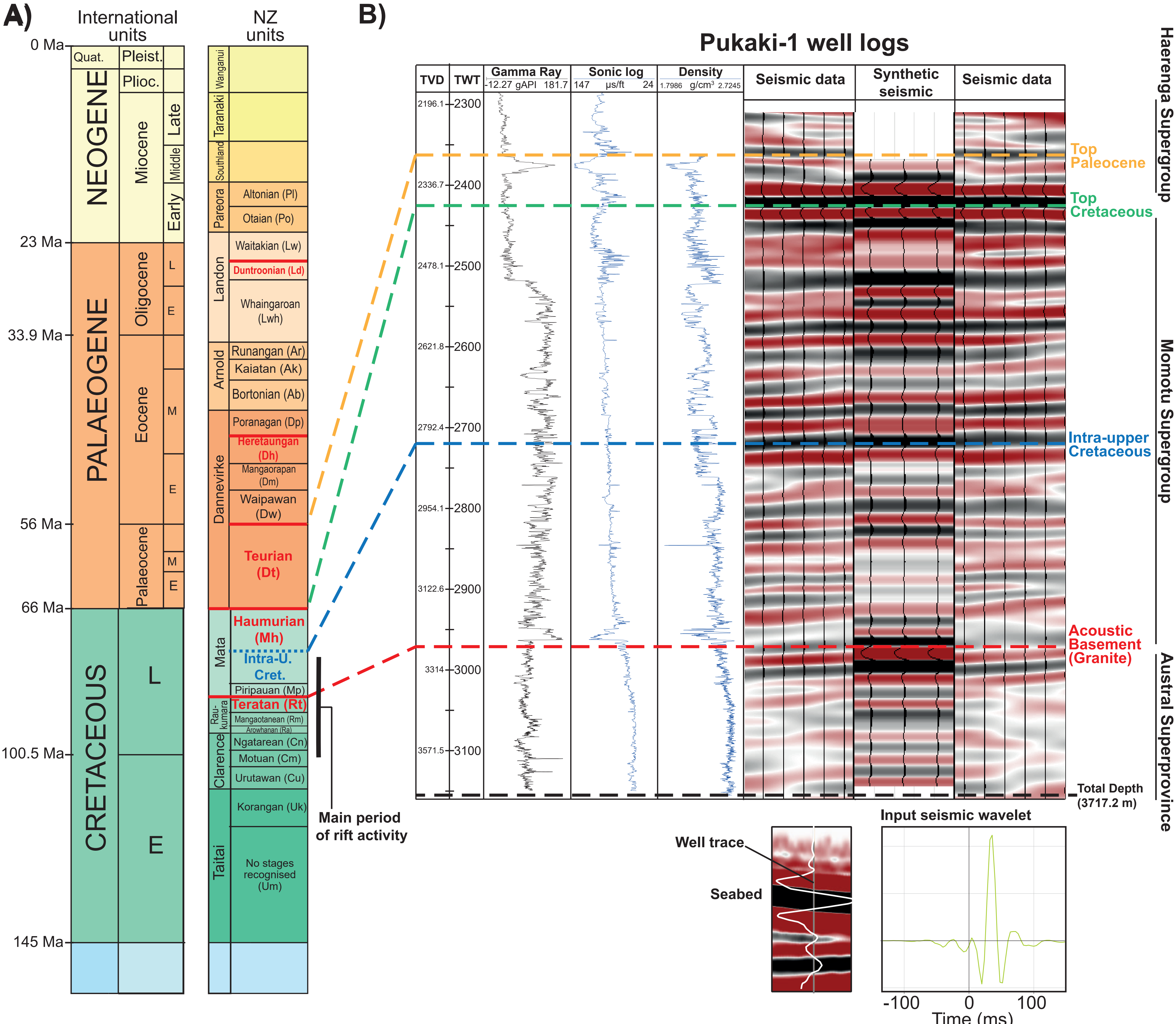
A)
International units
NZ units
0 Ma
23 Ma
33.9 Ma
56 Ma
66 Ma
100.5 Ma
145 Ma
Quat.
Pleist.
Plioc.
Miocene
Late
Middle
Early
NEOGENE
PALAEOGENE
Oligocene
Eocene
Palaeocene
CRETACEOUS
Wanganui
Taranaki
Southland
Pareora
Altonian (Pl)
Otaian (Po)
Landon
Waitakian (Lw)
Duntroonian (Ld)
Whaingaroan (Lwh)
Arnold
Runangan (Ar)
Kaiatan (Ak)
Bortonian (Ab)
Dannevirke
Poranagan (Dp)
Heretaungan (Dh)
Mangaorapan (Dm)
Waipawan (Dw)
Teurian (Dt)
Mata
Haumurian (Mh)
Intra-U. Cret.
Piripauan (Mp)
Raukumara
Teratan (Rt)
Mangaotanean (Rm)
Arowhanan (Ra)
Clarence
Ngatarean (Cn)
Motuan (Cm)
Urutawan (Cu)
Taitai
Korangan (Uk)
No stages recognised (Um)
Main period of rift activity
B)
Pukaki-1 well logs
TVD
TWT
Gamma Ray -12.27 gAPI 181.7
Sonic log 147 μs/ft 24
Density 1.7986 g/cm³ 2.7245
Seismic data
Synthetic seismic
Seismic data
2196.1 2300
2336.7 2400
2478.1 2500
2621.8 2600
2792.4 2700
2954.1 2800
3122.6 2900
3314 3000
3571.5 3100
Top Paleocene
Top Cretaceous
Intra-upper Cretaceous
Acoustic Basement (Granite)
Total Depth (3717.2 m)
Haerenga Supergroup
Momotu Supergroup
Austral Superprovince
Well trace
Seabed
Input seismic wavelet
-100
0
100
Time (ms)

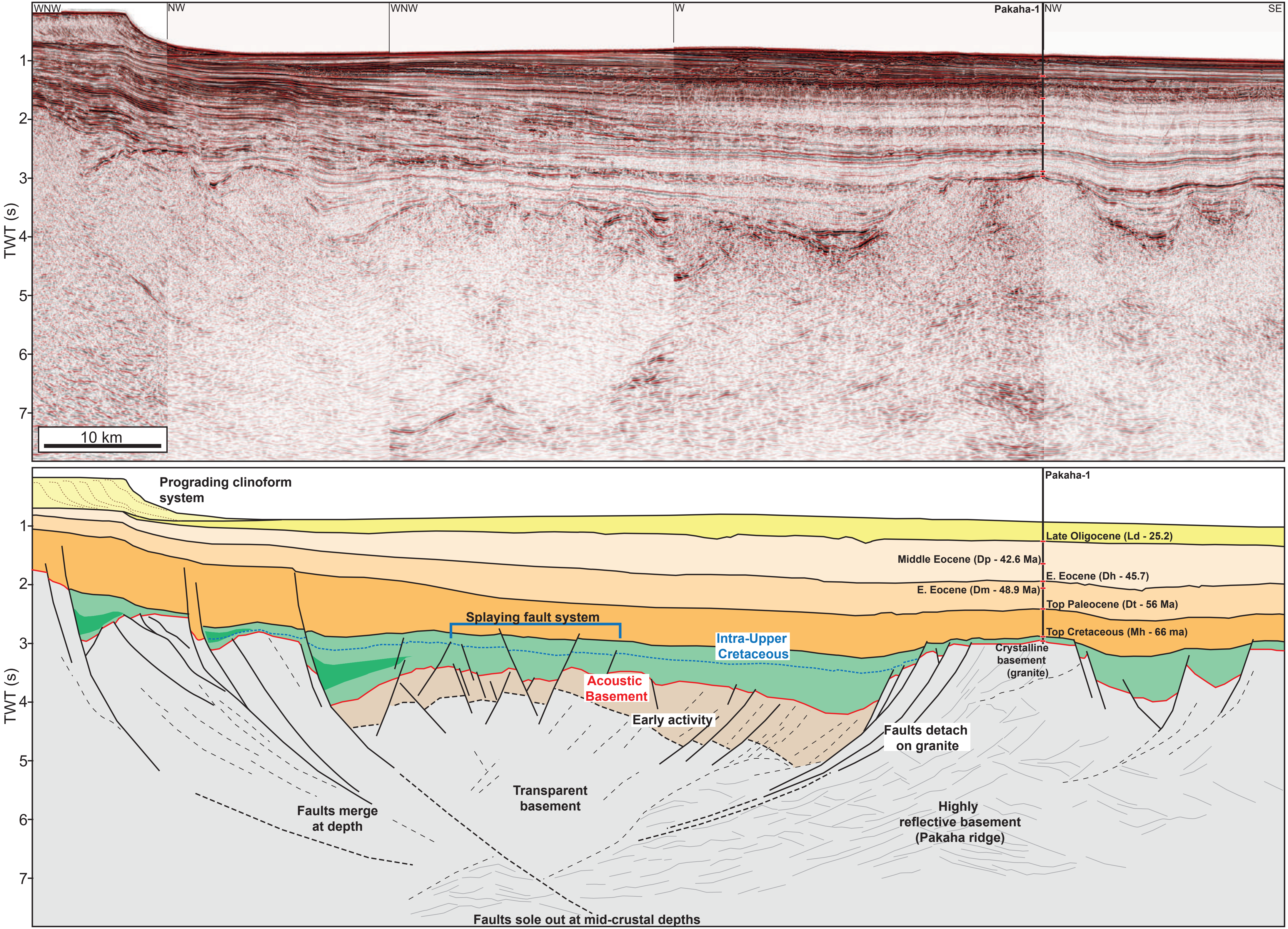

WNW
NW
WNW
W
Pakaha-1
NW
SE
TWT (s)
1
2
3
4
5
6
7
10 km
Prograding clinoform system
Pakaha-1
Late Oligocene (Ld - 25.2)
Middle Eocene (Dp - 42.6 Ma)
E. Eocene (Dh - 45.7)
E. Eocene (Dm - 48.9 Ma)
Top Paleocene (Dt - 56 Ma)
Splaying fault system
Top Cretaceous (Mh - 66 ma)
Intra-Upper Cretaceous
Crystalline basement (granite)
Acoustic Basement
Early activity
Faults detach on granite
Transparent basement
Faults merge at depth
Highly reflective basement (Pakaha ridge)
Faults sole out at mid-crustal depths

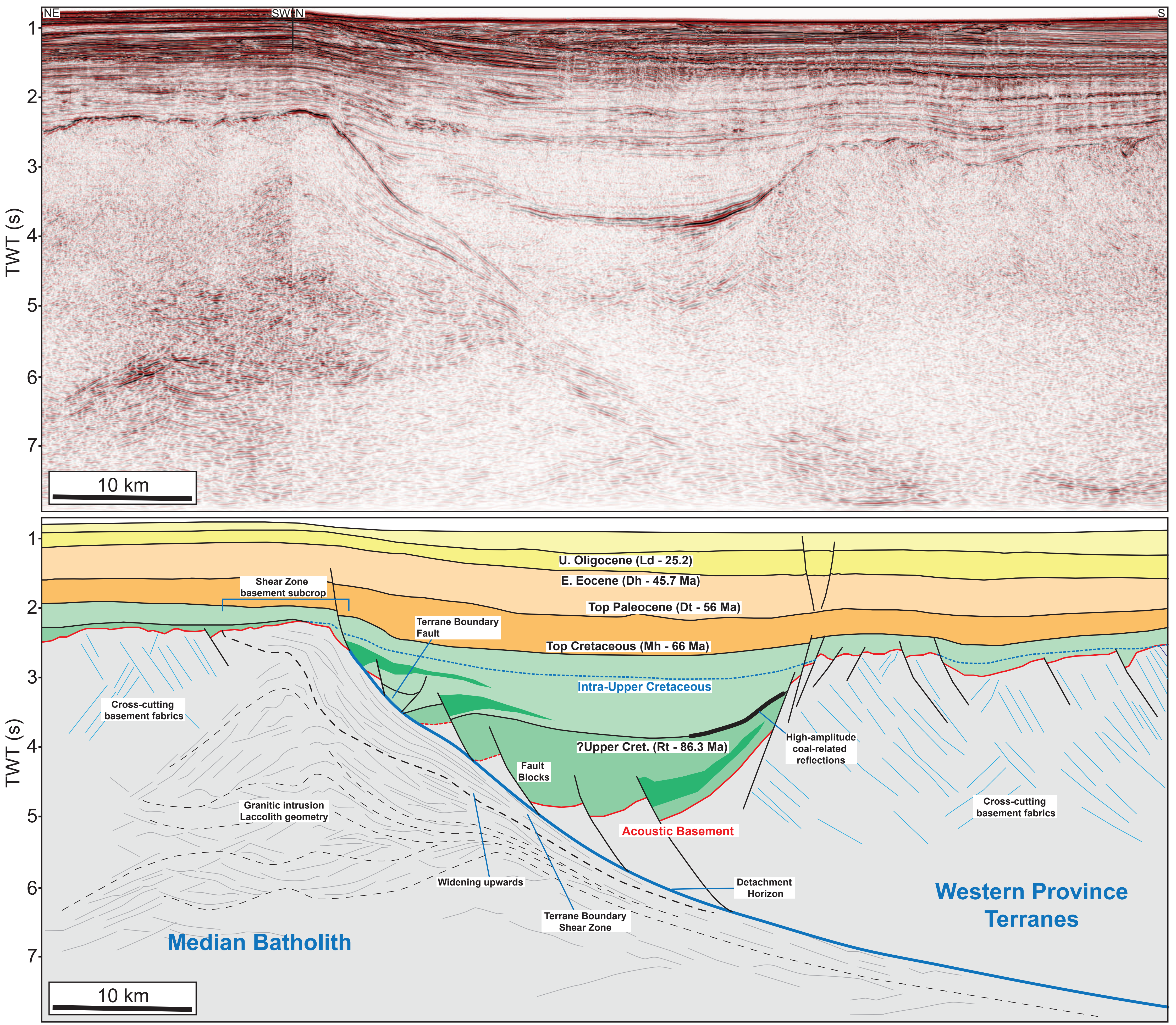

NE
SW
N
S
TWT (s)
10 km
U. Oligocene (Ld - 25.2)
E. Eocene (Dh - 45.7 Ma)
Top Paleocene (Dt - 56 Ma)
Top Cretaceous (Mh - 66 Ma)
Intra-Upper Cretaceous
?Upper Cret. (Rt - 86.3 Ma)
Shear Zone basement subcrop
Terrane Boundary Fault
Cross-cutting basement fabrics
High-amplitude coal-related reflections
Fault Blocks
Granitic intrusion Laccolith geometry
Acoustic Basement
Widening upwards
Detachment Horizon
Terrane Boundary Shear Zone
Western Province Terranes
Median Batholith

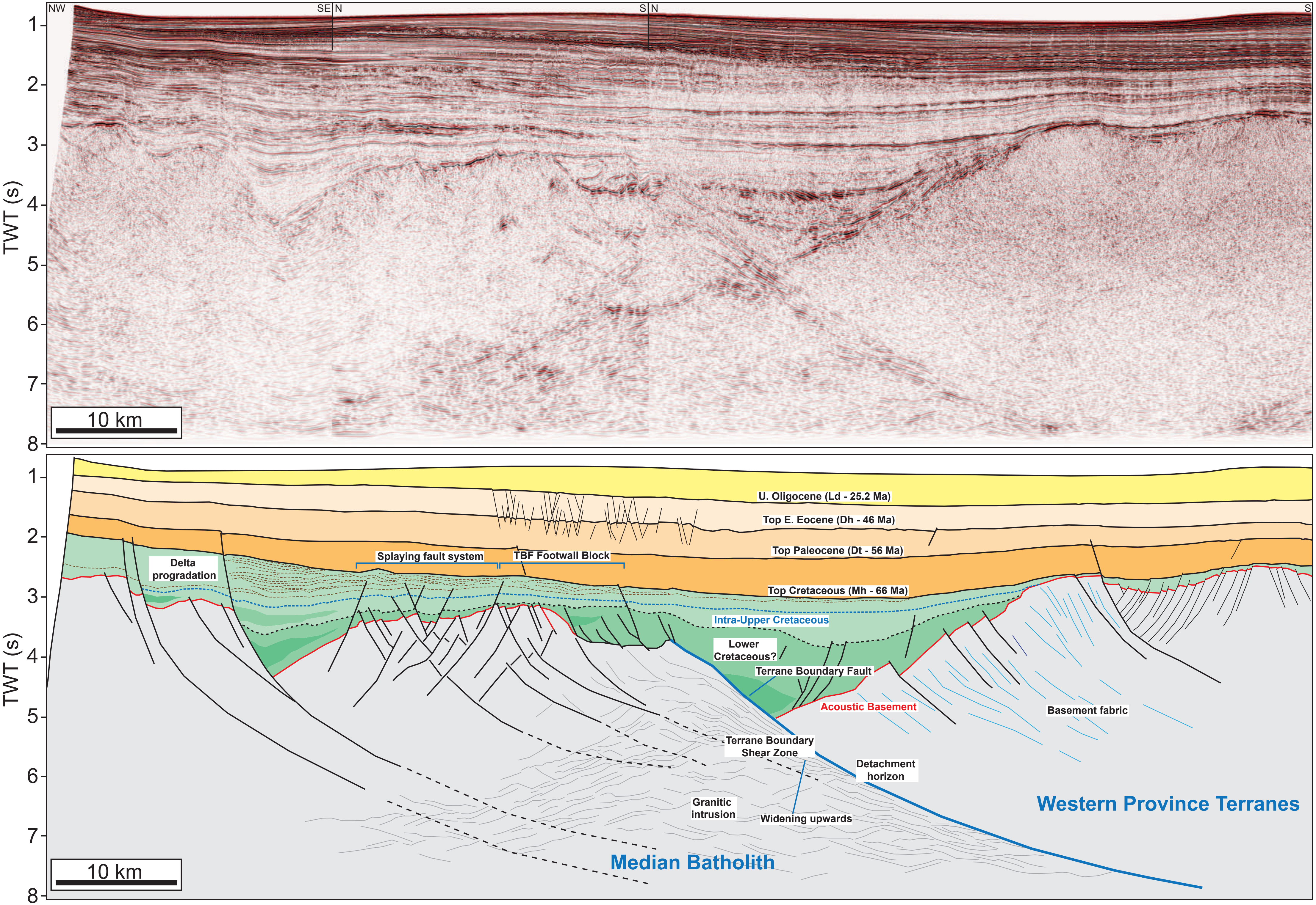
NW
SE
N
S
N
S
TWT (s)
10 km
U. Oligocene (Ld - 25.2 Ma)
Top E. Eocene (Dh - 46 Ma)
Top Paleocene (Dt - 56 Ma)
Top Cretaceous (Mh - 66 Ma)
Delta progradation
Splaying fault system
TBF Footwall Block
Intra-Upper Cretaceous
Lower Cretaceous?
Terrane Boundary Fault
Acoustic Basement
Basement fabric
Terrane Boundary Shear Zone
Detachment horizon
Granitic intrusion
Widening upwards
Western Province Terranes
Median Batholith

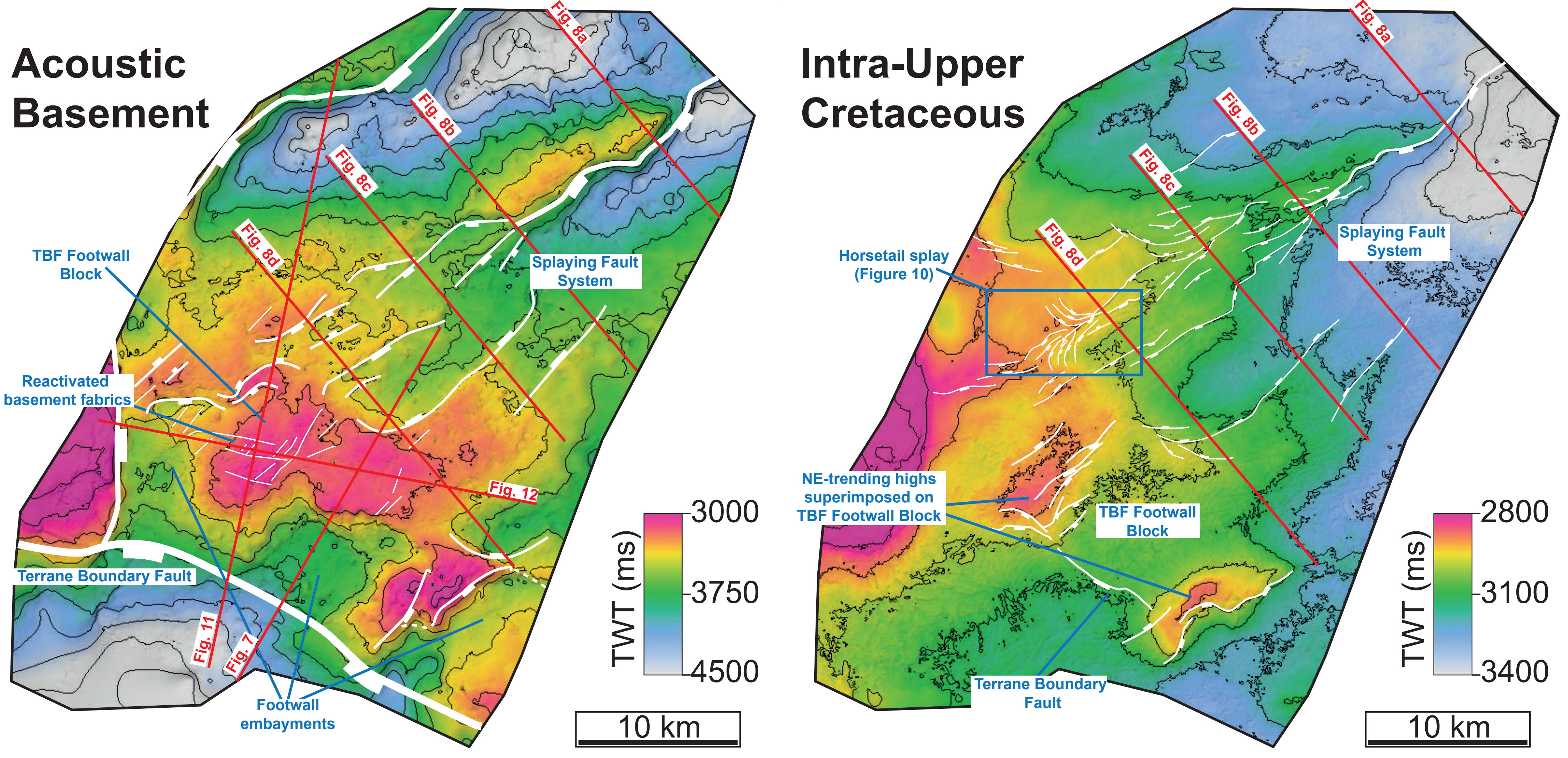

Acoustic Basement
Fig. 8a
Fig. 8b
Fig. 8c
Fig. 8d
TBF Footwall Block
Splaying Fault System
Reactivated basement fabrics
Fig. 12
Terrane Boundary Fault
Fig. 11
Fig. 7
Footwall embayments
3000
3750
4500
TWT (ms)
10 km
Intra-Upper Cretaceous
Fig. 8a
Fig. 8b
Fig. 8c
Fig. 8d
Horsetail splay (Figure 10)
Splaying Fault System
NE-trending highs superimposed on TBF Footwall Block
TBF Footwall Block
Terrane Boundary Fault
2800
3100
3400
TWT (ms)
10 km

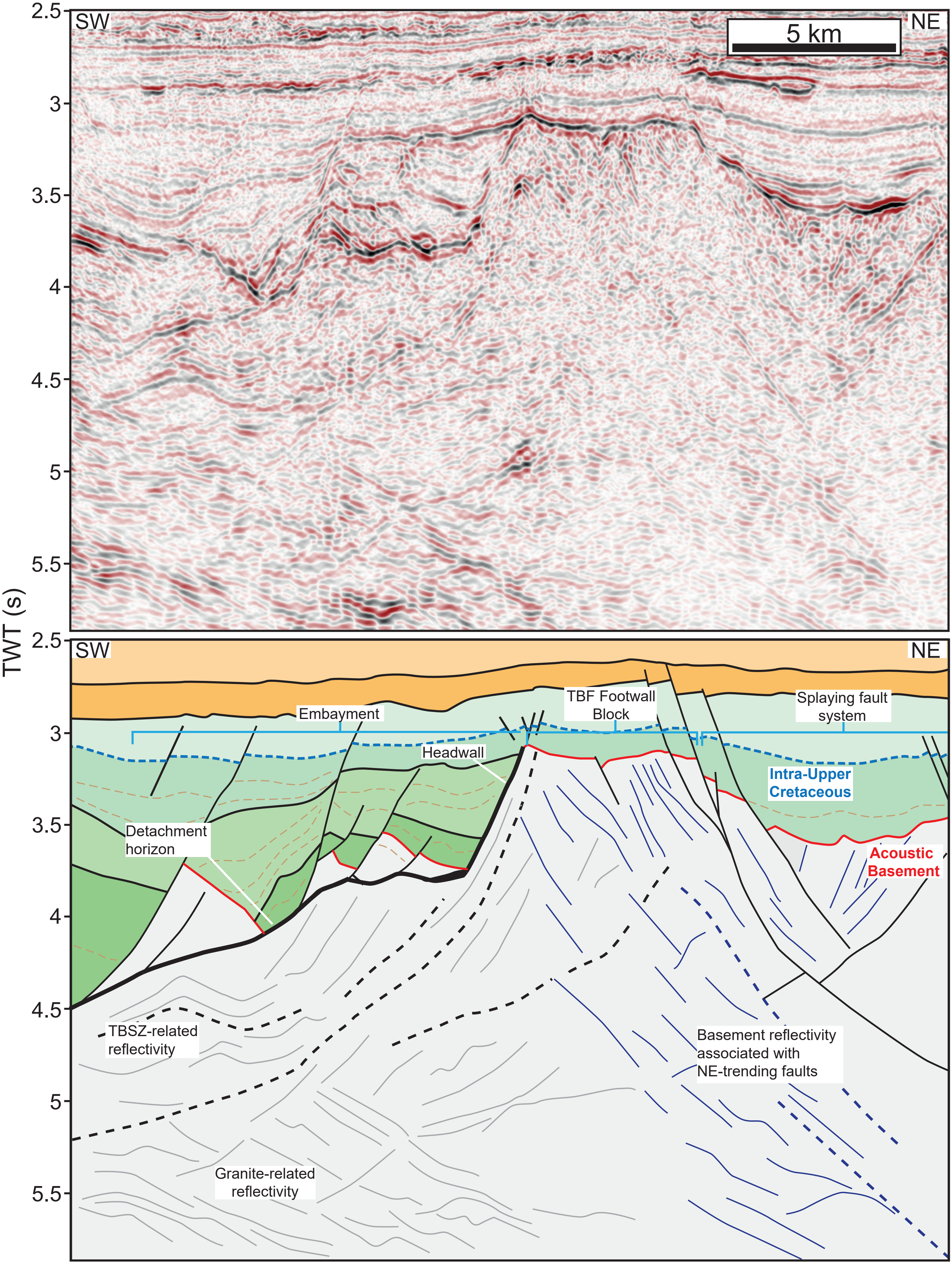

SW
NE
5 km
TWT (s)
2.5
3
3.5
4
4.5
5
5.5
Embayment
TBF Footwall
Block
Splaying fault
system
Headwall
Intra-Upper
Cretaceous
Detachment
horizon
Acoustic
Basement
TBSZ-related
reflectivity
Basement reflectivity
associated with
NE-trending faults
Granite-related
reflectivity

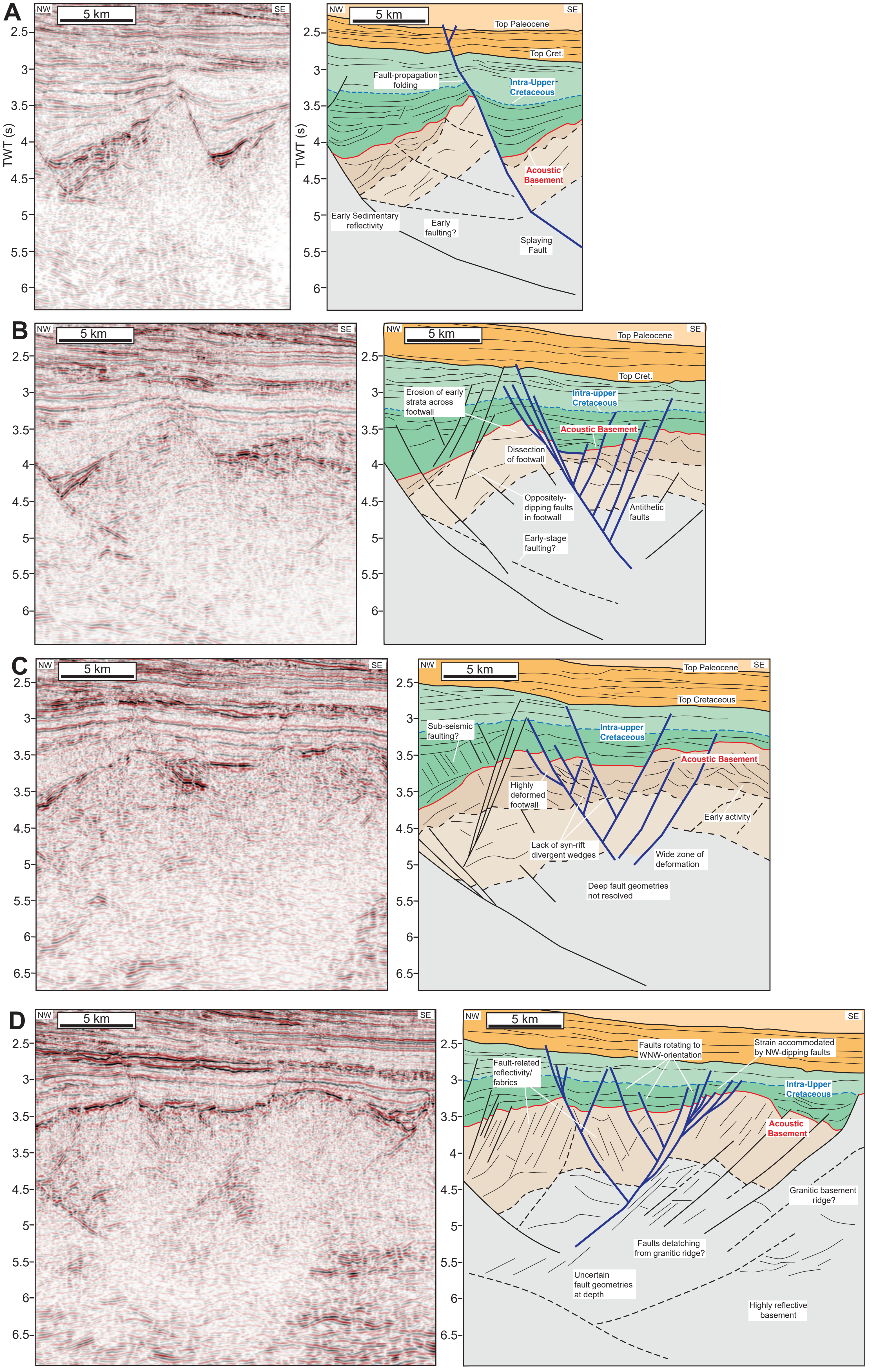
A
B
C
D
NW
SE
5 km
TWT (s)
Top Paleocene
Top Cret.
Fault-propagation folding
Intra-Upper Cretaceous
Acoustic Basement
Early Sedimentary reflectivity
Early faulting?
Splaying Fault
Top Paleocene
Top Cret.
Erosion of early strata across footwall
Intra-upper Cretaceous
Acoustic Basement
Dissection of footwall
Oppositely-dipping faults in footwall
Antithetic faults
Early-stage faulting?
Top Paleocene
Top Cretaceous
Sub-seismic faulting?
Intra-upper Cretaceous
Acoustic Basement
Highly deformed footwall
Early activity
Lack of syn-rift divergent wedges
Wide zone of deformation
Deep fault geometries not resolved
Faults rotating to WNW-orientation
Strain accommodated by NW-dipping faults
Fault-related reflectivity/ fabrics
Intra-Upper Cretaceous
Acoustic Basement
Granitic basement ridge?
Faults detaching from granitic ridge?
Uncertain fault geometries at depth
Highly reflective basement

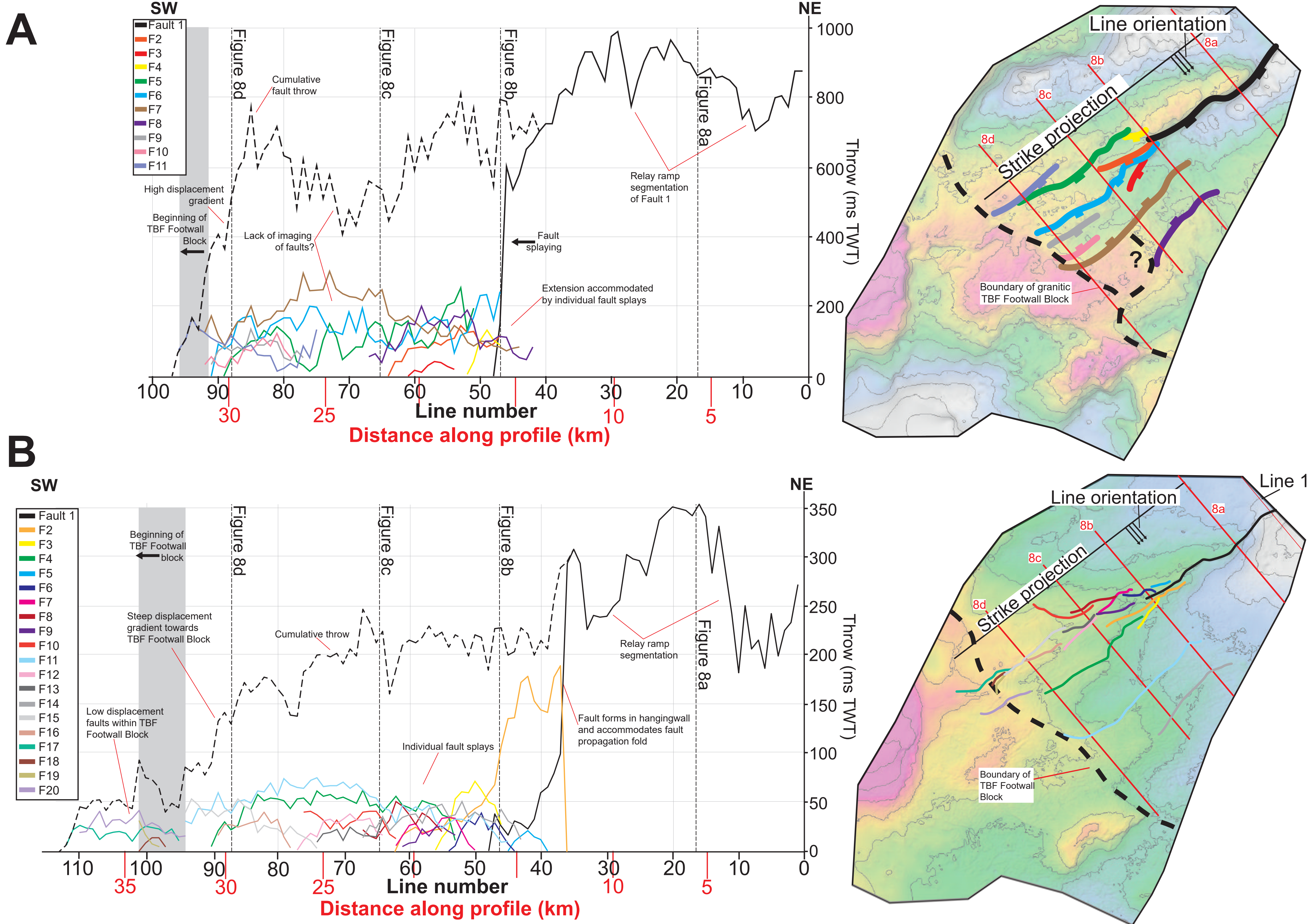
A
SW
NE
Fault 1
F2
F3
F4
F5
F6
F7
F8
F9
F10
F11
Figure 8d
Figure 8c
Figure 8b
Figure 8a
Cumulative fault throw
High displacement gradient
Beginning of TBF Footwall Block
Lack of imaging of faults?
Fault splaying
Extension accommodated by individual fault splays
Relay ramp segmentation of Fault 1
Throw (ms TWT)
Line number
Distance along profile (km)
Line orientation
Strike projection
Boundary of granitic TBF Footwall Block
8a
8b
8c
8d
?
B
SW
NE
Fault 1
F2
F3
F4
F5
F6
F7
F8
F9
F10
F11
F12
F13
F14
F15
F16
F17
F18
F19
F20
Beginning of TBF Footwall block
Steep displacement gradient towards TBF Footwall Block
Low displacement faults within TBF Footwall Block
Cumulative throw
Individual fault splays
Fault forms in hangingwall and accommodates fault propagation fold
Relay ramp segmentation
Throw (ms TWT)
Line number
Distance along profile (km)
Line 1
Line orientation
Strike projection
Boundary of TBF Footwall Block
8a
8b
8c
8d

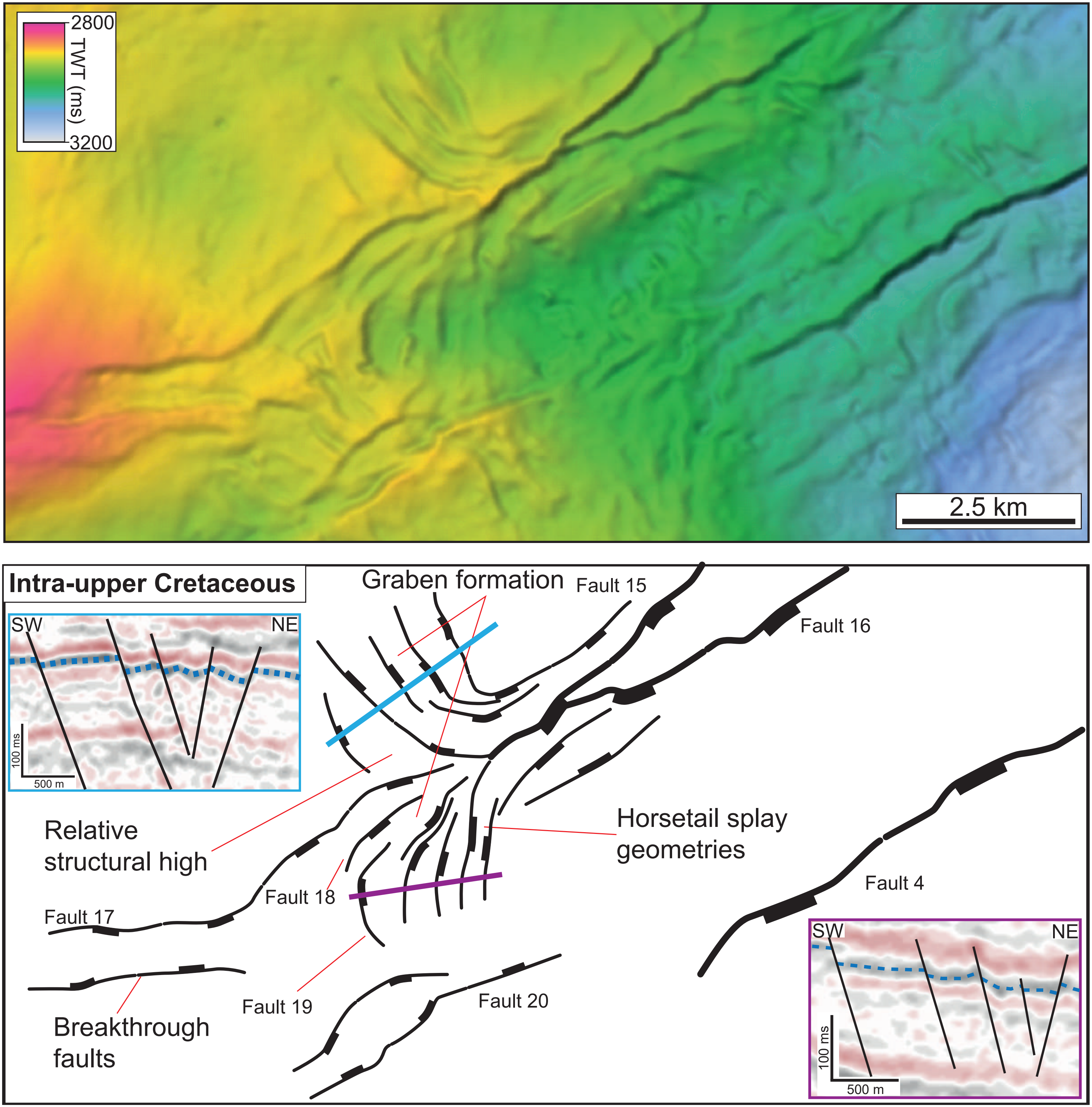
2800
TWT (ms)
3200
2.5 km
Intra-upper Cretaceous
Graben formation
Fault 15
Fault 16
SW
NE
100 ms
500 m
Relative
structural high
Horsetail splay
geometries
Fault 4
Fault 17
Fault 18
Fault 19
Fault 20
Breakthrough
faults
SW
NE
100 ms
500 m

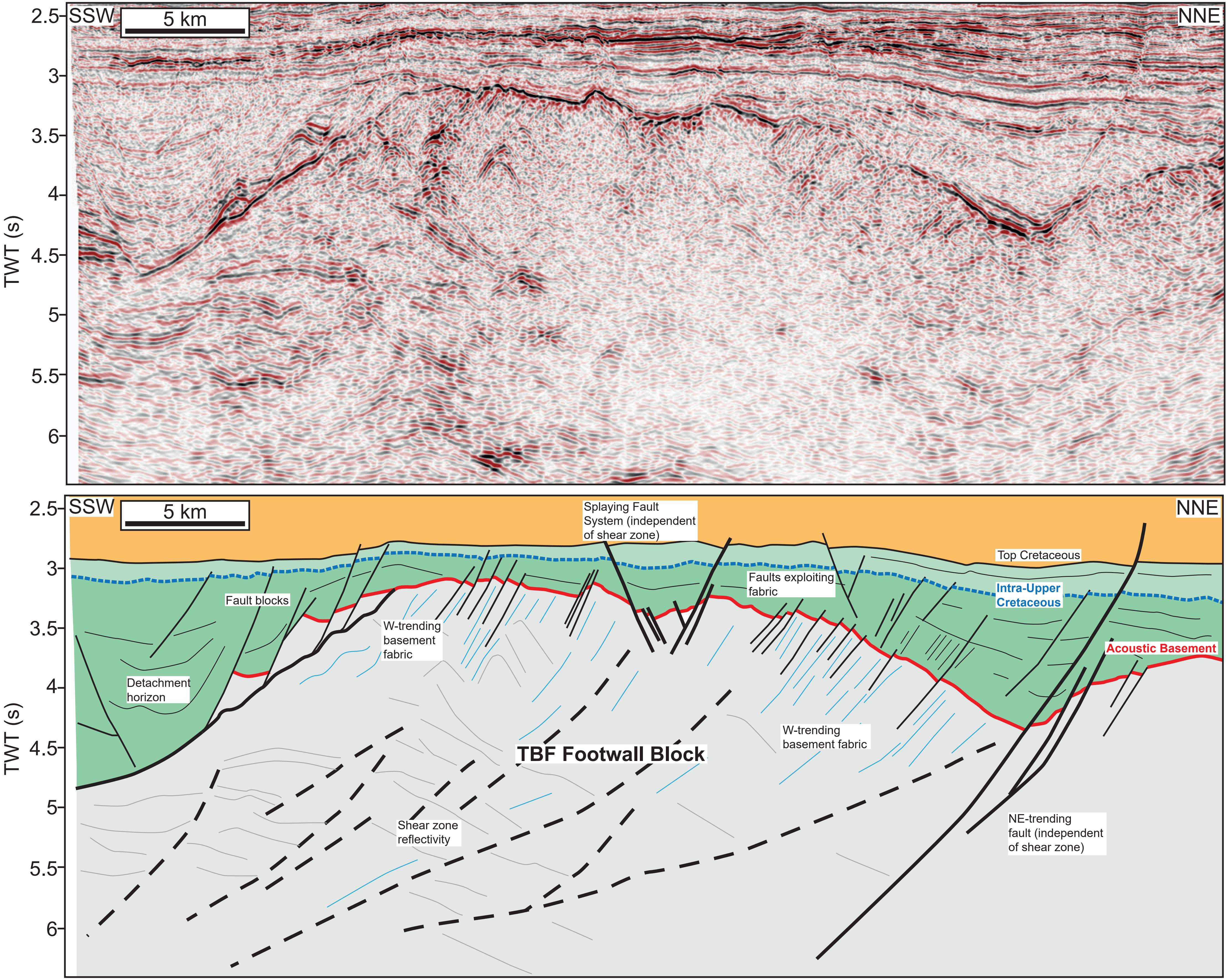

SSW
5 km
NNE
TWT (s)
2.5
3
3.5
4
4.5
5
5.5
6
Splaying Fault System (independent of shear zone)
Top Cretaceous
Faults exploiting fabric
Intra-Upper Cretaceous
Fault blocks
W-trending basement fabric
Acoustic Basement
Detachment horizon
TBF Footwall Block
W-trending basement fabric
Shear zone reflectivity
NE-trending fault (independent of shear zone)

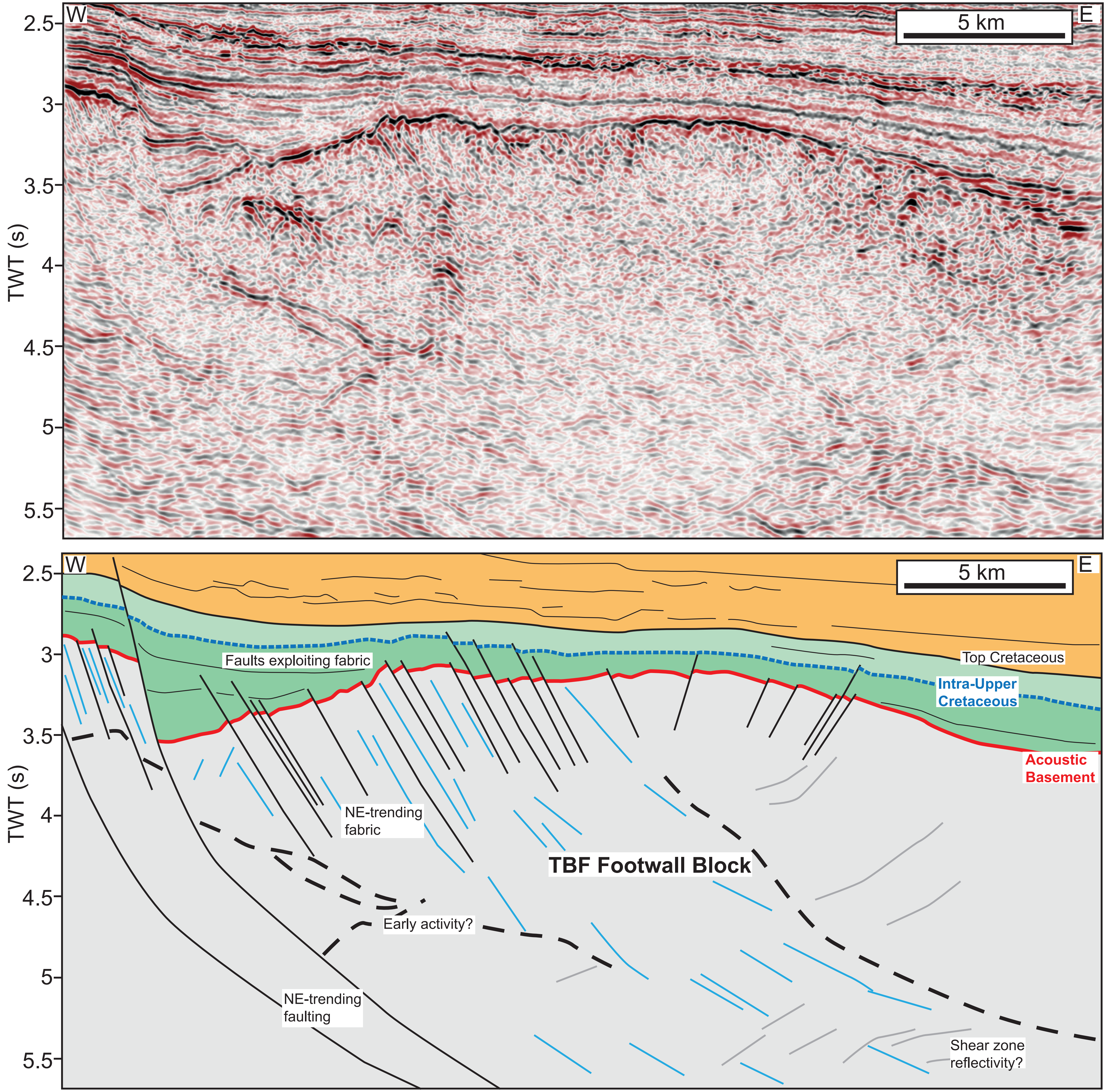

W
E
5 km
TWT (s)
2.5
3
3.5
4
4.5
5
5.5
Faults exploiting fabric
Top Cretaceous
Intra-Upper Cretaceous
Acoustic Basement
NE-trending fabric
TBF Footwall Block
Early activity?
NE-trending faulting
Shear zone reflectivity?

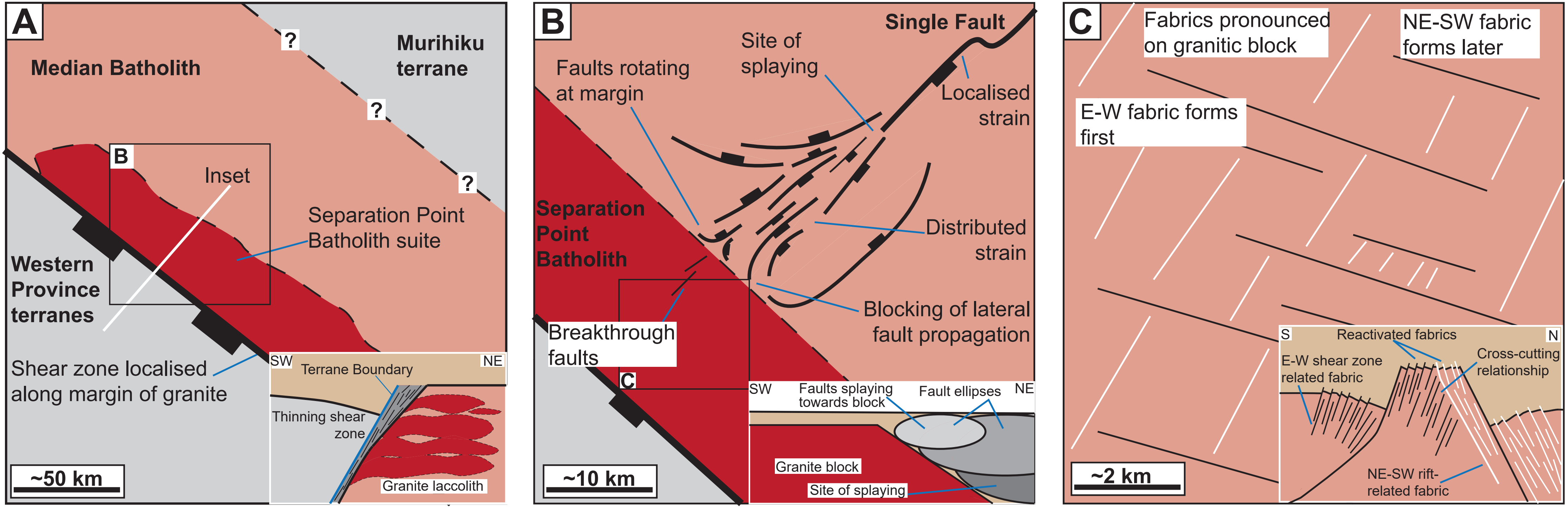

A
Median Batholith
Murihiku terrane
?
?
?
B
Inset
Separation Point Batholith suite
Western Province terranes
Shear zone localised along margin of granite
SW
NE
Terrane Boundary
Thinning shear zone
Granite laccolith
~50 km
B
Single Fault
Site of splaying
Faults rotating at margin
Localised strain
Separation Point Batholith
Distributed strain
Blocking of lateral fault propagation
Breakthrough faults
C
SW
NE
Faults splaying towards block
Fault ellipses
Granite block
Site of splaying
~10 km
C
Fabrics pronounced on granitic block
NE-SW fabric forms later
E-W fabric forms first
S
N
Reactivated fabrics
E-W shear zone related fabric
Cross-cutting relationship
NE-SW rift-related fabric
~2 km

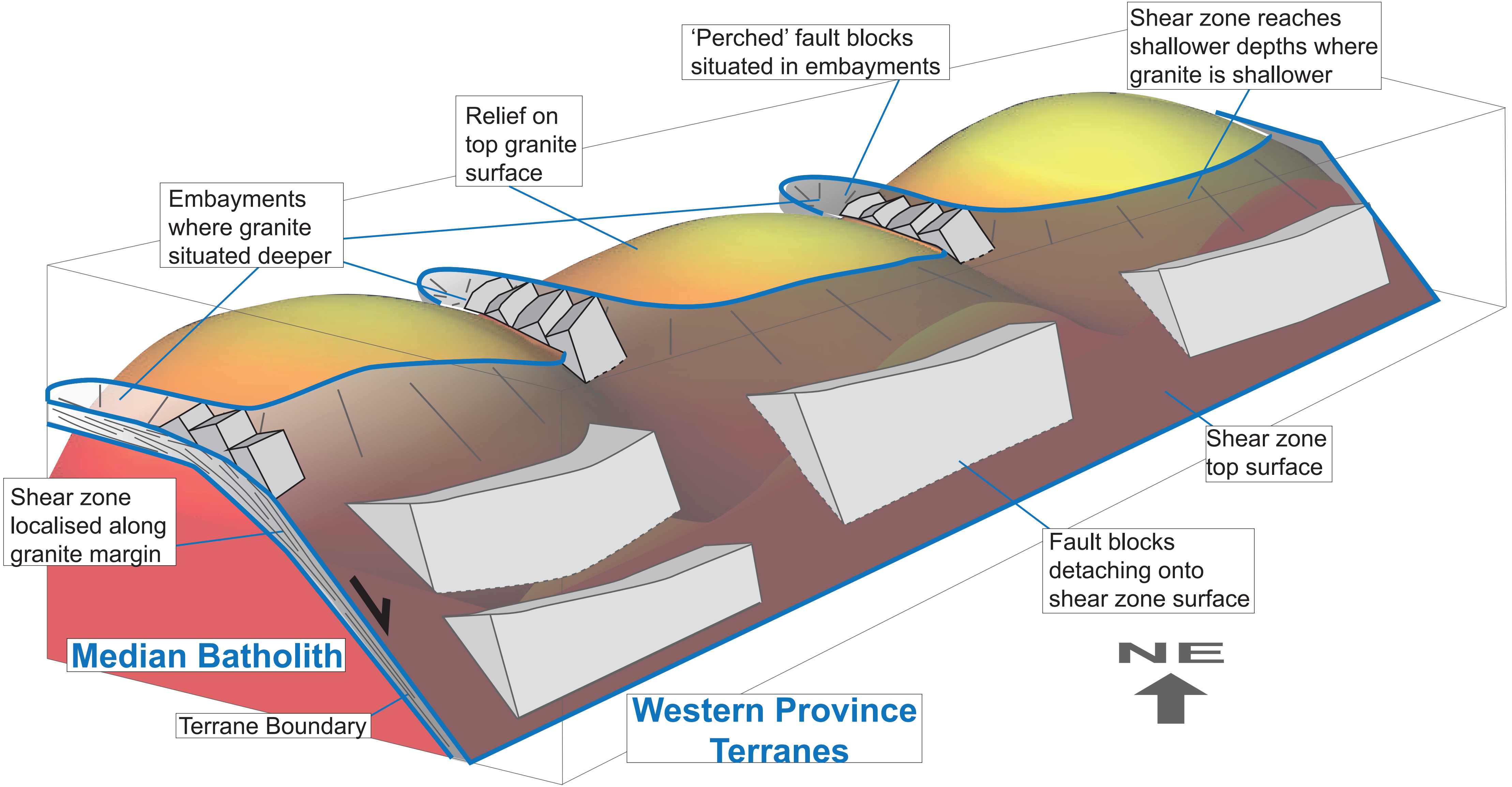
Shear zone reaches shallower depths where granite is shallower
'Perched' fault blocks situated in embayments
Relief on top granite surface
Embayments where granite situated deeper
Shear zone localised along granite margin
Median Batholith
Terrane Boundary
Western Province Terranes
Shear zone top surface
Fault blocks detaching onto shear zone surface
NE

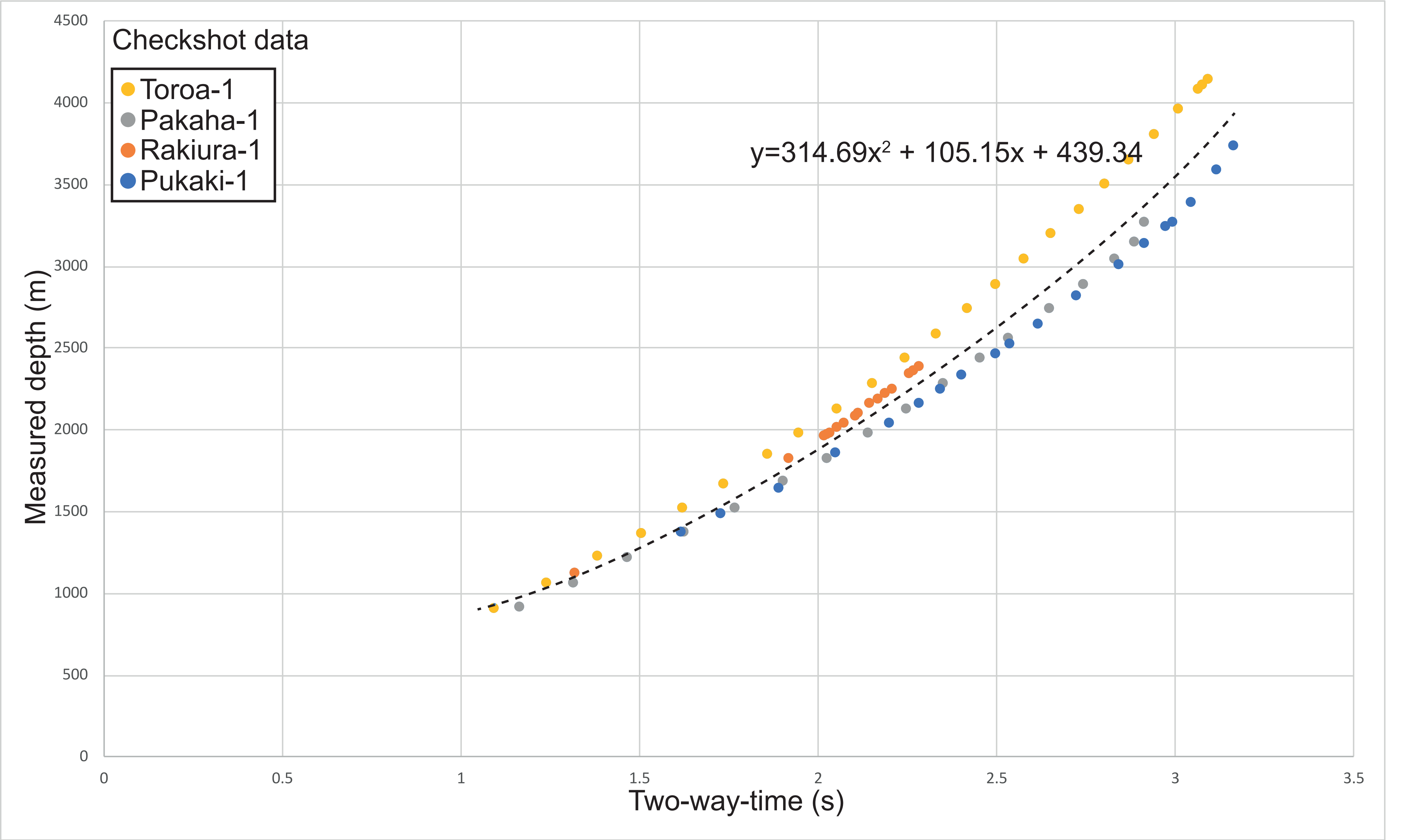
Checkshot data
Toroa-1
Pakaha-1
Rakiura-1
Pukaki-1
y=314.69x² + 105.15x + 439.34
Measured depth (m)
Two-way-time (s)
4500
4000
3500
3000
2500
2000
1500
1000
500
0
0
0.5
1
1.5
2
2.5
3
3.5